CHEMISTRY
A EUROPEAN JOURNAL

DOI: 10.1002/chem.200700219

Organometallic Polymers Assembled from Cation–π Interactions: Use of Ferrocene as a Ditopic Linker Within the Homologous Series $[\{(Me_3Si)_2NM\}_2\cdot(Cp_2Fe)]_\infty$ (M = Na, K, Rb, Cs; Cp = cyclopentadienyl)

J. Jacob Morris,[a] Bruce C. Noll,[a] Gordon W. Honeyman,[b] Charles T. O'Hara,[b] Alan R. Kennedy,[b] Robert E. Mulvey,[b] and Kenneth W. Henderson*[a]

Abstract: Addition of ferrocene to solutions of alkali metal hexamethyldisilazides M(HMDS) in arenes (in which M = Na, K, Rb, Cs) allows the subsequent crystallization of the homologous series of compounds $[\{(Me_3Si)_2NM\}_2\cdot(Cp_2Fe)]_\infty$ (**1**–**4**). Similar reactions using LiHMDS led to the recrystallization of the starting materials. The crystal structures of **1**–**4** reveal the formation of one-dimensional chains composed of dimeric $[\{M(HMDS)\}_2]$ aggregates, which are bridged through neutral ferrocene molecules by η^5-cation–π interactions. In addition, compounds **3** and **4** also contain interchain agostic M···C interactions, producing two-dimensional 4^4-nets. Whereas **1** and **2** were prepared from toluene, the syntheses of **3** and **4** required the use of *tert*-butylbenzene as the reaction media. The attempted crystallization of **3** and **4** from toluene resulted in formation of the mixed toluene/ferrocene solvated complexes $[\{(Me_3Si)_2NM)_2\}_2\cdot(Cp_2Fe)_x\cdot(Tol)_y]_\infty$ (in which M = Rb, x = 0.6, y = 0.8, **5**; M = Cs, x = 0.5, y = 1, **6**). The extended solid-state structures of **5** and **6** are closely related to the 4^4-sheets **3** and **4**, but are now assembled from a combination of cation–π, agostic, and π–π interactions. The charge-separated complex $[K\{(C_6H_6)_2Cr\}_{1.5}(Mes)][Mg(HMDS)_3]$ (**15**) was also structurally characterized and found to adopt an anionic two-dimensional 6^3-network through doubly η^3-coordinated bis(benzene)chromium molecules. DFT calculations at the B3LYP/6–31G* level of theory indicate that the binding energies of both ferrocene and toluene to the M(HMDS) dimers increases in the sequence Li < Na < K. This pattern is a consequence of the larger metals allowing more open coordination spheres to support cation–π contacts. By comparison, binding of the isolated metal cations to the aromatic groups follow the reverse order K < Na < Li. A combined analysis of theoretical and experimental data suggest that ferrocene is a stronger cation–π donor than toluene for the lighter metals, but that this difference is eliminated on descending the group.

Keywords: alkali metals · metallocenes · noncovalent interactions · pi interactions · self-assembly

Introduction

The interaction between alkali metal cations and the π-face of neutral aromatic systems has emerged as an important binding force in a diverse range of biological and chemical settings.[1–4] For example, cation–π interactions are believed to play a key role in numerous biological recognition processes,[5] such as the binding of acetylcholine to proteins,[6,7] the functioning of ion channels within cell membranes,[8–10] and the stabilization of tertiary protein structure.[11] In turn, a number of model arene-derivatized receptor systems such as cyclophanes,[12,13] collarenes,[14] macrocyclic polyethers,[15] tripodal pyrazoles,[16,17] and zeolites[18] have been employed to study the binding of alkali metal ions. Complementary investigations examining the ability of host systems incorporating alkali metals to coordinate neutral arene molecules have similarly been completed.[4] Cation–π interactions also play a critical role in determining the course of many reactions involving s-block metal reagents,[19–22] and their presence has been exploited in various materials chemistry applications,[23–27] such as the preparation of ultrathin nanotubes.[28]

[a] J. J. Morris, Dr. B. C. Noll, Dr. K. W. Henderson
Department of Chemistry and Biochemistry
University of Notre Dame, Notre Dame, Indiana 46556–5670 (USA)
Fax: (+1) 574-631-6652
E-mail: khenders@nd.edu

[b] Dr. G. W. Honeyman, Dr. C. T. O'Hara, Dr. A. R. Kennedy, Dr. R. E. Mulvey
WestCHEM, Department of Pure and Applied Chemistry
University of Strathclyde, Glasgow, Scotland G1 1XL (UK)

We became interested in cation–π interactions during our recent work focusing on the incorporation of s-block metals in metal–organic frameworks.[29] Specifically, we have demonstrated that an assortment of s-block metal cage aggregates may be linked through ditopic Lewis base linkers to form one-, two-, and three-dimensional networks.[29a–c] The formation of coordination polymers through the combination of unsaturated metal centers and polytopic donor ligands has been one of the most successful strategies adopted in the preparation of extended structures.[30–36] In addition to coordinative bonding, a multitude of interactions have been used in the synthesis of periodic networks including covalent bonding,[37] hydrogen bonding,[38–40] π–π interactions,[41–43] ionic interactions,[44,45] lipophilic interactions,[46,47] metal–metal interactions,[48–50] and halogen bonding.[51,52] However, the deliberate use of cation–π interactions to control the assembly of extended networks has received little attention.

Our objective was to utilize ferrocene, the prototypical metallocene, as a neutral, linear, ditopic π-linker to bridge between preformed alkali metal aggregates. Somewhat surprisingly, there is only a single example of a structurally characterized compound in which an alkali metal is bound to the π-face of ferrocene.[53] In 2004 Mulvey reported the synthesis of the charge-separated, molecular complex $[K{\cdot}(Cp_2Fe)_2{\cdot}(Tol)_2]^+[Mg(HMDS)_3]^-$, in which a single potassium cation is coordinated by two η^5-ferrocene and two η^3-toluene molecules (Figure 1).

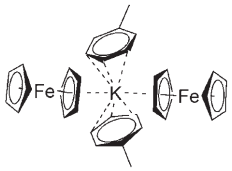

Figure 1. Cationic moiety of $[K{\cdot}(Cp_2Fe)_2{\cdot}(Tol)_2]^+[Mg(HMDS)_3]^-$.

Moreover, only two examples of ferrocene acting as a bridging ligand through its π-faces to build polymers have appeared, namely the double sandwich ferrocene adduct of trimeric perfluoro-*ortho*-phenylenemercury reported by Gabbai,[54] and the mixed Ga^I/Ga^{III} complex $[(Cp_2Fe){\cdot}(Ga_2Cl_4)]_\infty$, reported by Wagner (Figure 2).[55] Very recently the Wagner group have extended this work to utilize a 1,1′-bis(pyrazol-1-yl)borate-substituted ferrocene derivative to coordinate to the alkali metals.[56] Taking a broader view, only a handful of complexes between alkali metal cations and homoleptic cyclopentadienyl metallocenes have been structurally characterized. The most notable contributions are from the groups of Stalke and Wright,[57–62] who have shown that various oligomers or extended structures may be formed by the combination of alkali metal cyclopentadienyls and neutral metallocenes. In addition, there are a small number of substituted metallocene derivatives that are known to coordinate to alkali metal cations.[63]

We selected the alkali metal hexamethyldisilazides (M-(HMDS); M = Li, Na, K, Rb, Cs) for study as they combine

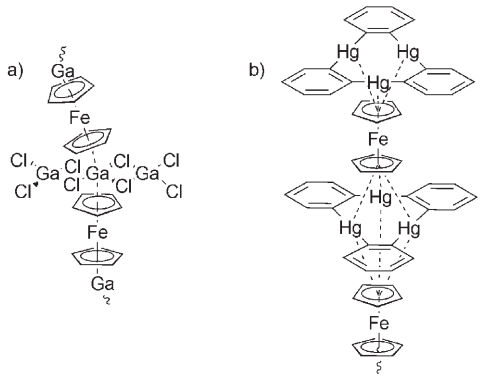

Figure 2. Sections of the ferrocene-bridged polymers a) $[(Cp_2Fe){\cdot}(Ga_2Cl_4)]_\infty$ and b) $[(Cp_2Fe){\cdot}\{(o\text{-}C_6F_4Hg)_3\}_2]_\infty$.

several attractive features: 1) they are all known to form dimeric M_2N_2 ring structures upon solvation with appropriate Lewis bases,[64–75] 2) they are soluble in arene media without the need for the addition of donor solvents, and 3) both KHMDS and CsHMDS crystallize as bis(η^6-toluene)-solvated dimers, demonstrating their ability to support cation–π interactions.[72,75] Overall, it was envisioned that ferrocene would act as a ditopic linker to create one-dimensional chains of dimers in each case.

Herein, we report the successful completion of this work through the synthesis and structural characterization of the compounds $[\{(Me_3Si)_2NM\}_2{\cdot}(Cp_2Fe)]_\infty$, in which M = Na (**1**), K (**2**), Rb (**3**), Cs (**4**). This group is a unique example of a homologous series for alkali-metal amides.[76] The structural similarities within this set of compounds enables an unusually detailed examination of cation–π interactions in the absence of complicating factors, such as differing solvation of the metals and variations in aggregation state. Furthermore, the remarkable mixed toluene/ferrocene complexes $[\{(Me_3Si)_2NM\}_2{\cdot}(Cp_2Fe)_x{\cdot}(Tol)_y]_\infty$ (M = Rb, $x = 0.6$, $y = 0.8$ (**5**); M = Cs, $x = 0.5$, $y = 1$ (**6**)) were discovered during the course of our studies. The unexpected formation and structures of these complexes provide further insights into cation–π interactions. Finally, a density functional theory (DFT) computational study has been completed and is used to further investigate the nature of the bonding in these compounds, and provide comparative information on the binding of ferrocene and toluene.

Results and Discussion

Synthesis and spectroscopic analysis: Initial attempts to prepare the complexes involved dissolution of the individual metal amides LiHMDS, NaHMDS, KHMDS, RbHMDS and CsHMDS in toluene, followed by mixing with 0.5 molar equivalents of ferrocene. In the case of NaHMDS this resulted in the instant formation of a precipitate, which dissolved on vigorous heating. All of the other reactions remained as yellow-orange solutions. High-quality crystals were grown from each of the solutions after individually op-

timizing their concentrations and temperatures for crystal growth.

Repeated reactions involving LiHMDS consistently led to the precipitation of uncomplexed ferrocene and/or LiHMDS (as determined by NMR spectroscopy and single-crystal X-ray diffraction). This is presumably due to insufficient space being available within lithium atom's coordination sphere for solvation by ferrocene. Further support for this conjecture is provided by computational modeling (see later).

^{1}H NMR analyses in [D_6]benzene of the crystals produced from the reactions involving NaHMDS and KHMDS each displayed single HMDS and ferrocene resonances in a 1:0.5 ratio, suggestive of polymer formation, that is, $[\{(Me_3Si)_2NM\}_2\cdot(Cp_2Fe)]_\infty$, in which M = Na (**1**), K (**2**). Although the ^{1}H NMR spectra of the crystals obtained from the reactions involving RbHMDS and CsHMDS also indicated single HMDS and ferrocene resonances, they were accompanied by signals clearly arising from toluene, in an approximate ratio of 1:0.25:0.5. The use of single crystals for the NMR analyses produced similar spectra, excluding the possibility of coprecipitation of separately solvated toluene and ferrocene complexes. In turn, single-crystal XRD studies confirmed the presence of both toluene and ferrocene in each crystal, and the structures refined as $[\{(Me_3Si)_2NRb\}_2\cdot(Cp_2Fe)_{0.6}\cdot(Tol)_{0.8}]_\infty$ (**5**) and $[\{(Me_3Si)_2NCs\}_2\cdot(Cp_2Fe)_{0.5}\cdot(Tol)_1]_\infty$ (**6**). In an attempt to overcome the problem of co-solvation the media for crystallization was altered from toluene to *tert*-butylbenzene, the idea being that increasing the steric bulk of the arene would inhibit its interaction with the metals. This approach proved successful, allowing the crystallization of the complexes $[\{(Me_3Si)_2NM\}_2\cdot(Cp_2Fe)]_\infty$, in which M = Rb (**3**), Cs (**4**), containing 1:0.5 ratios of amide to ferrocene.

In all instances the chemical shift positions within the ^{1}H and ^{13}C NMR spectra obtained for **1**–**6** in [D_6]benzene were identical to those of uncomplexed ferrocene and the individual metal amides. A variable-temperature study of the NaHMDS/ferrocene system **1** between 20 and −60 °C in [D_8]toluene similarly showed a single set of peaks with identical chemical shift positions to those of the individual compounds. The NMR spectra obtained from crystals of **1** dissolved in the non-coordinating solvent [D_{12}]cyclohexane were also identical to those of ferrocene and metal amide. UV/Vis studies in toluene and in *tert*-butylbenzene, and cryoscopic studies in benzene were also consistent with no discernable interaction between the metal amides and ferrocene in solution. Solid-state infra-red spectroscopic studies of **1**–**4** did show some effects of ferrocene complexation. These results will be discussed in the computational section, as useful comparisons can be made with the calculated structures.

Crystallographic studies: Following characterization of their composition by NMR spectroscopy, the crystal structures of the complexes **1**–**6** were subsequently completed. A comparison of selected bond lengths and angles for compounds **1**–**6** is detailed in Table 1.

The solid-state structures of **1**–**4** are composed of dimeric M_2N_2 rings connected through doubly η^5-coordinated ferrocene molecules to form 1D polymeric chains (Figures 3 and 4). The formation of M_2N_2 ring dimers was anticipated as this is the most commonly found aggregation state for monodentate solvates of the alkali metal hexamethyldisilazides (Table 2).[66–70,72–75] As expected, the metrical parameters within the dimeric units for each compound are very similar to those of the comparable solvates. The M−N and the Si−N distances in **1**–**4** all lie within the range of bond lengths found for the previously characterized dimeric complexes. Also, the Si-N-Si angles for **1**–**4** match the trend seen for the solvated structures, in which this angle increases by 1–5° for the sodium and potassium complexes with respect to the unsolvated aggregates, whereas it decreases by 1–3° for the rubidium and cesium complexes.

Due to rotational disorder of the cyclopentadienyl rings the C−C distances were fixed at 1.420 Å in all of the complexes. The bonding between the iron centers and the carbon atoms within the ferrocene units of **1**–**4** differs slightly from that found in uncomplexed ferrocene.[77] In particular, the Fe−C distances in simple ferrocene lie in the narrow range 2.010–2.063 Å, whereas those of **1**–**4** cover a slightly wider range of 1.985(4)–2.106(3) Å. The Fe−$Cp_{centroid}$ distance in ferrocene is 1.650 Å, which is close to the values of 1.643, 1.644, 1.647, and 1.652 Å in **1**–**4**, respectively. Consequently, participation in cation–π bonding has minor but noticeable effects on the bonding within the ferrocene molecules.

Next, considering the interaction between ferrocene and the alkali metals it is clear that the cyclopentadienyl rings are essentially η^5-bound in each complex, with the M−C distances varying by <0.15 Å within each complex. The distance between the alkali metal and the centroid of the cyclopentadienyl ring increases as the group is descended, with mean M−$Cp_{centroid}$ distances of 2.791, 2.931, 3.228 and 3.335 Å for **1**–**4**, respectively. The apparent discontinuity between the potassium and rubidium complexes is explained by changing from in-plane to tilted positions by the ferrocene molecules (see later).

The most closely related arene-solvated analogues of **1**–**4** are the toluene complexes $[(Me_3Si)_2NK\cdot(Tol)]_2$ (**7**)[72] and $[\{(Me_3Si)_2NCs\}_2\cdot(Tol)]_\infty$ (**8**).[75] Complex **7** is a simple molecular dimer, with terminal toluene molecules η^6-bound to the metal centers. In comparison, complex **8** forms a 1D polymer in which the toluene molecules bridge between the metal centers. In both **7** and **8** the M−$Tol_{centroid}$ distances are noticeably longer at 2.976 and 3.455 Å, respectively, than those of the ferrocene complexes **2** and **4**, at 2.931 and 3.335 Å, respectively. Also, of relevance is the previously mentioned complex $[K\cdot(Cp_2Fe)_2\cdot(Tol)_2]^+[Mg(HMDS)_3]^-$ (**9**)[53] in which single potassium centers coordinate in a η^5 fashion to two terminal ferrocene molecules and η^3 to two toluene molecules (Figure 5). Similar to **7** and **8**, the K−$Tol_{centroid}$ distance in **9** is longer at 3.143 Å than the K−$Cp_{centroid}$ distance of 2.964 Å. These values suggest that ferrocene is acting as a stronger donor to the metal centers,

Table 1. Key bond lengths [Å] and angles [°] for **1**–**6**.

	1 (M = Na)	**2** (M = K)	**3** (M = Rb)	**4** (M = Cs)	**5** (M = Rb)	**6** (M = Cs)
M–N	2.399(1)	2.740(2)	2.894(2)	3.035 (2)	2.943(2)	3.056(2)
			2.972(2)	3.130(2)	3.019(2)	3.149(2)
Si–N	1.688(1)	1.667(2)	1.666(2)	1.666(2)	1.692(2)	1.669(2)
			1.669(2)	1.666(2)	1.693(2)	1.670(2)
$M–C_{Ferro}$	2.974(4)	3.112(3)	3.395(4)	3.496(7)	3.507(6)	3.549(7)
	2.979(6)	3.169(3)	3.397(4)	3.505(8)	3.525(6)	3.558(6)
	3.063(7)	3.172(3)	3.464(3)	3.557(10)	3.530(5)	3.617(5)
	3.068(6)		3.468(4)	3.571(10)	3.558(6)	3.631(6)
	3.119(4)		3.509(3)	3.603(12)	3.561(6)	3.667(6)
$M–Cp_{centroid}$	2.791	2.931	3.228	3.335	3.323	3.396
$M–C_{Tol}$					3.369(7)	3.530(5)
					3.423(6)	3.561(5)
					3.449(7)	3.563(5)
					3.554(5)	3.625(5)
					3.579(5)	3.627(4)
					3.630(4)	3.658(4)
$M–Tol_{centroid}$					3.214	3.315
$Fe–C_{Ferro}$	1.985(4)	2.001(3)	2.023(3)	2.034(9)	2.035(5)	2.050(6)
	2.021(6)	2.004(4)	2.030(4)	2.035(7)	2.049(5)	2.053(6)
	2.024(5)	2.106(3)	2.043(3)	2.051(11)	2.051(5)	2.063(5)
	2.080(3)		2.053(4)	2.052(7)	2.073(4)	2.067(5)
	2.082(6)		2.061(3)	2.062(9)	2.074(5)	2.074(6)
N-M-N	99.37(6)	96.09(9)	94.08(5)	93.47(5)	94.46(5)	94.05(4)
M-N-M	80.63(6)	83.91(9)	85.92(5)	86.53(5)	85.54(5)	85.95(4)
Si-N-M	106.49(3)	108.03(6)	104.84(8)	103.27(8)	104.50(7)	102.58(8)
	113.90(3)		107.68(9)	107.84(9)	107.98(8)	107.90(8)
			109.24(8)	109.72(8)	109.46(7)	110.01(8)
			113.44(9)	112.32(8)	113.67(8)	112.58(8)
Si-N-Si	126.27(10)	130.8(2)	127.23(11)	128.35(11)	127.05(10)	128.51(11)
$M-M-Cp_{centroid}$	180.00	180.00	148.59	148.04	150.05	149.16

likely as a consequence of its smaller size and also perhaps due to its greater electron-donating ability. In this regard it should be remembered that although ferrocene is neutral, the cyclopentadienyl rings are formally anionic.

Of note here is the series of compounds prepared by Wagner $[\{Na(Fcpz)\}\cdot\{Na(DME)_3\}]_\infty$ (**10**) and $[M_2(Fcpz)\cdot(DME)_3]_\infty$, M = K (**11**), Rb (**12**), Cs (**13**), in which the 1,1′-bis(pyrazol-1-yl)borate-substituted ferrocene ligand $[1,1'\text{-}Fc(BMe_2pz)_2]^{2-}$ (Fc = $(C_5H_4)_2Fe$, pz = pyrazolyl) forms polymers in association with the alkali metals.[56b] In these compounds the metals coordinate to the π-faces of the cyclopentadienyl groups, but are further stabilized through dative M–N(pyrazolyl) bonds, as well as by contacts with the added Lewis base 1,2-dimethoxyethane. In **10** the sodium centers are solvated by two pyrazolyl units from separate ferrocene molecules to create anionic chains of $[Na(Fcpz)^-]_\infty$ (Figure 5a). The anionic chains are charged balanced by isolated $Na(DME)_3^+$ ions. The structures of **11**–**13** differ from **10** in that they are composed of linear columns of dimeric metal–pyrazolyl units (M_2N_2), with one metal solvated by two DME molecules, whereas the second metal is solvated by a single DME and by two separate cyclopentadienyl units (Figure 5b).

Of particular interest is the comparison between the metal–π bonding in **1**–**4** and **10**–**13**. The mean $Na–Fc_{centroid}$ distance in **10** is 2.576 Å, which is 0.22 Å shorter than the $Na–Cp_{centroid}$ distance in **1**. In contrast, the mean $K–Fc_{centroid}$ distance in **11** is 3.263 Å, which is 0.33 Å longer than the $K–Cp_{centroid}$ distance in **2**. In comparison, **3** and **4** have metal–Cp bonds that vary by <0.05 Å relative to the complexes **12** and **13**. These inconsistent changes in metal–Cp distances reveal an interesting pattern of bonding within this set of compounds. First, they demonstrate that the cation–π interactions have significant flexibility in terms of metal–Cp distances. The shorter distances in the sodium complex **10** relative to **1** are likely a consequence of repulsive interactions

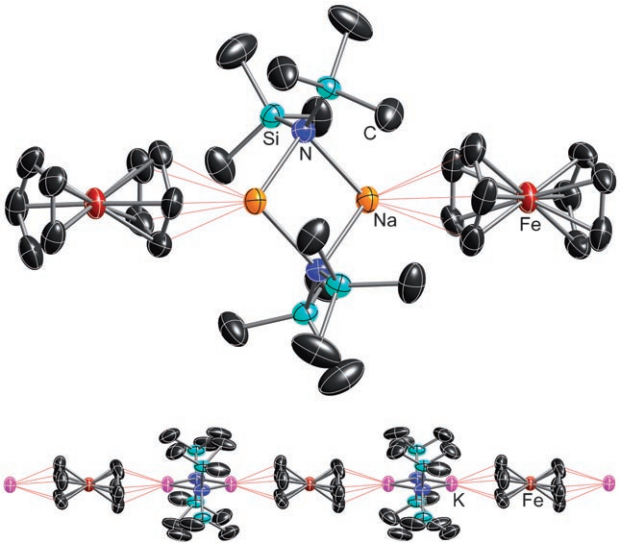

Figure 3. Top: Section of the polymeric structure of **1** highlighting the dimeric Na_2N_2 ring core η^5-coordinated to two ferrocene molecules. Bottom: Extended section of **2** showing the linear polymeric chain structure. Hydrogen atoms are omitted for clarity.

between the HMDS units of the dimer and the solvating ferrocenes. This is in accord with the inability of LiHMDS to complex to ferrocene, and is supported by our computational studies (see later). Next, the decrease in the potassium–Cp distances in **2** relative to **11** are understandable as the metal centers are additionally solvated in the latter compound by didentate DME molecules. Also, the larger size of potassium in comparison to sodium allows for a more open coordination sphere at the metal centers of the dimer. Finally, it appears that the bond lengths surrounding the larger rubidium and cesium ions are influenced to a smaller degree by the additional solvation of DME present in **12** and **13**.

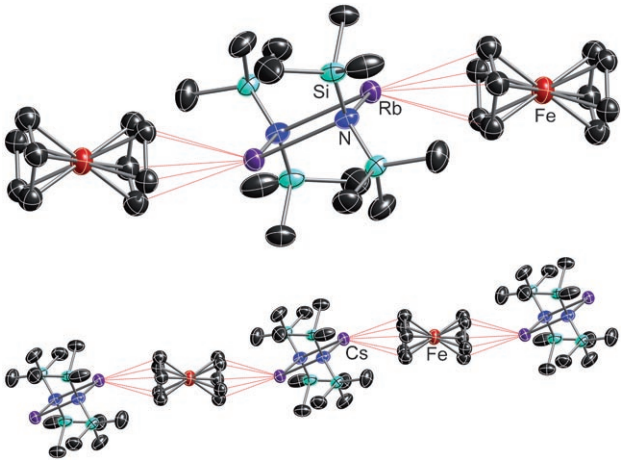

Figure 4. Top: Section of the polymeric structure of **3** highlighting the dimeric Rb_2N_2 ring core η^5-coordinated to two ferrocene molecules in a tilted fashion. Bottom: Extended section of **4** showing the zigzag polymeric chain structure. Hydrogen atoms are omitted for clarity.

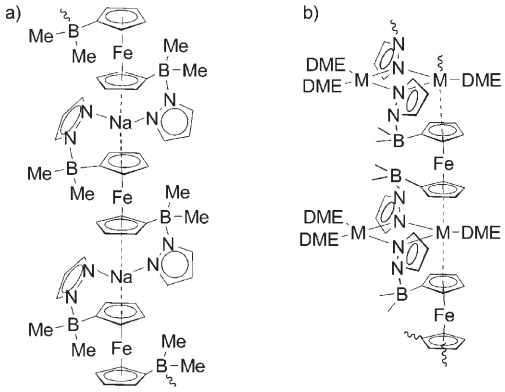

Figure 5. Sections of the polymeric structures of a) $[Na(Fcpz)]^-_\infty$ (**10**), and b) $[M_2(Fcpz)\cdot(DME)_3]_\infty$, M = K (**11**), Rb (**12**), Cs (**13**).

Table 2. Comparison of selected bond lengths [Å] and angles [°], for M(HMDS) (M = Na, K, Rb, Cs) compounds.

Compound	Aggregate	M–N	Si–N	Si-N-Si	Reference
sodium compounds					
$[(Me_3Si)_2NNa]_\infty$	polymer	2.352(2), 2.358(3)	1.687(2), 1.694(2)	125.6(1)	[64]
$[(Me_3Si)_2NNa]_3$	trimer	2.358(8)–2.394(8)	1.680(8)–1.706(8)	124.6(4)–126.2(4)	[65]
$[\{(Me_3Si)_2NNa\}_2\cdot(C_4H_8O)_2]$	dimer	2.398(2), 2.399(2)	1.677(2), 1.673(2)	129.6(1)	[66]
$[\{(Me_3Si)_2NNa\}\cdot(C_4H_8O_2)_2]_\infty$	polymer (linked monomers)	2.380(1)	1.673(2)	130.8(1)	[67]
$[(Me_3Si)_2NNa\cdot(C_9H_{18}NO)]_2$	dimer	2.382(3)–2.408(3)	1.681(3)–1.687(3)	126.2(1), 127.6(1)	[68]
$[\{(Me_3Si)_2NNa\}_2\cdot(C_7H_{18}N_2)]_\infty$	polymer (linked dimers)	2.430(4), 2.425(4)	1.683(4), 1.682(4)	124.5(2)	[69]
$[(Me_3Si)_2NNa\cdot(C_5H_9N)]_2$	dimer	2.379(3)–2.403(3)	1.679(3)–1.689(3)	126.1(1), 126.6(1)	[70]
potassium compounds					
$[(Me_3Si)_2NK]_2$	dimer	2.770(3), 2.803(3)	1.678(3), 1.685(3)	129.2(2)	[71]
$[(Me_3Si)_2NK\cdot(Tol)]_2$	dimer	2.745(3), 2.801(3)	1.671(3), 1.677(3)	133.8(2)	[72]
$[(Me_3Si)_2NK\cdot(C_{10}H_{20}N_2)]_2$	dimer	2.763(1), 2.843(1)	1.669(1), 1.669(1)	136.0(1)	[73]
$[\{(Me_3Si)_2NK\}\cdot(C_4H_8O_2)_2]_\infty$	polymer (linked monomers)	2.70(2)	1.64(1)	136.2(1)	[74]
rubidium compounds					
$[(Me_3Si)_2NRb]_2$	dimer	2.878(2), 2.956(2)	1.672(2), 1.677(2)	130.7(1)	[75]
$[\{(Me_3Si)_2NRb\}_2\cdot(C_4H_8O_2)_3]_\infty$	polymer (linked dimers)	2.946(6), 3.141(6)	1.652(6), 1.677(6)	129.5(4)	[67]
cesium compounds					
$[(Me_3Si)_2NCs]_2$	dimer	3.074(2), 3.149(2)	1.671(2), 1.674(2)	129.4(1)	[75]
$[\{(Me_3Si)_2NCs\}_2\cdot(Tol)]_\infty$	polymer (linked dimers)	3.016(3), 3.139(3)	1.673(3), 1.679(3)	128.0(2)	[75]
$[\{(Me_3Si)_2NCs\}_2\cdot(C_4H_8O_2)_3]_\infty$	polymer (linked dimers)	3.067(1), 3.388(2)	1.672(2), 1.673(2)	128.4(1)	[67]

Moving on to consider the extended supramolecular structures, in both **1** and **2** ferrocene acts as a ditopic linker, bridging between the dimeric aggregates to give isostructural one-dimensional polymers (Figure 3). In each compound the ferrocenes lie in the plane of the M_2N_2 dimeric rings (M-M-$Cp_{centroid}$ = 180.00°) to give completely linear chain structures. There are only a few examples of NaHMDS or KHMDS polymers. These include monomeric fragments of NaHMDS and KHMDS bridged by 1,4-dioxane to give three-dimensional networks,[67,74] and the dimeric aggregate of NaHMDS coordinated by bridging *N*,*N*,*N*′,*N*′-tetramethylpropanediamine, which adopts a one-dimensional chain structure.[69] The three known solvated structures of RbHMDS and CsHMDS all adopt polymeric structures. The 1,4-dioxane solvates adopt three-dimensional networks composed of linked M_2N_2 dimeric aggregates,[67] and the toluene solvate of CsHMDS forms a one-dimensional chain polymer as previously discussed.[75]

The structures of **3** and **4** are also isostructural one-dimensional chain polymers of M_2N_2 dimers bridged through ferrocene. However, the extended networks are more complex than those of **1** and **2**. As shown in Figure 4, the ferrocenes in **3** and **4** are tilted out of the M_2N_2 ring planes, with M-M-$Cp_{centroid}$ angles of 148.59° and 148.04° for **3** and **4**, respectively. This leads to the polymeric chains adopting an unusual zigzag conformation. The metals are involved in a number of close intra- and intermolecular agostic interactions not seen in **1** or **2**. For both compounds there are three close intramolecular M–$C_{(HMDS)}$ interactions of 3.499, 3.674, and 3.681 Å for **3**, and 3.629, 3.714, and 3.818 Å for **4** (metallic radii of 2.48 and 2.65 Å for Rb and Cs, and van der Waals radius of 1.70 Å for C). In addition, each metal also has a close intermolecular M–$C_{(HMDS)}$ contact to a neighboring chain within the crystalline lattice (3.505 Å for **3** and 3.602 Å for **4**). Indeed, these interchain agostic interactions are responsible for pushing the ferrocene ligands out of the M_2N_2 ring planes to give zigzag rather than linear polymers. Considering these agostic interactions the extended structures of **3** and **4** may be regarded as two-dimensional 4^4-nets, with the metal amide dimers occupying the corners of the square windows (Figure 6).

During our initial attempts to crystallize **3** and **4**, toluene was chosen as the solvent medium, since it was successfully used in the crystallization of **1** and **2**. Unexpectedly, it was discovered that toluene was present within the crystals in addition to ferrocene. Single-crystal X-ray studies identified the mixed-solvate structures $[\{(Me_3Si)_2NRb\}_2\cdot(Cp_2Fe)_{0.6}\cdot(Tol)_{0.8}]_\infty$ (**5**) and $[\{(Me_3Si)_2NCs\}_2\cdot(Cp_2Fe)_{0.5}\cdot(Tol)_1]_\infty$ (**6**). Analysis of the isostructural compounds **5** and **6** revealed dimeric M_2N_2 aggregates, for which the metal centers coordinate to either toluene or ferrocene (Figure 7). The two components were modeled separately and allowed to refine with partial site occupancies. The Cp ring has a slightly larger site occupancy of 59.5(6)% for **5** and an essentially equal site occupancy of 49.5(6)% for **6**. A check of multiple crystals for **5** and **6** gave replicable site occupancies for the ferrocene and toluene. Since the iron can only exist in the structure when the Cp ring is present, the site occupancy of the iron was fixed to match that of the Cp ring.

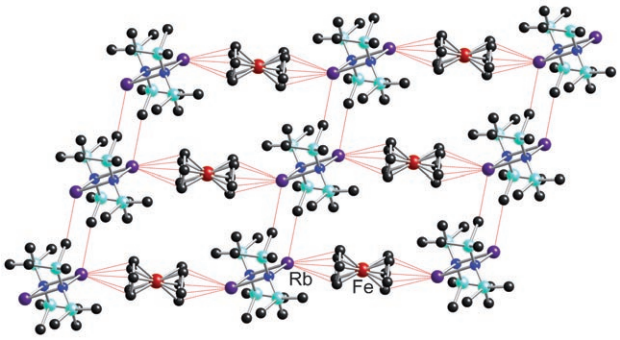

Figure 6. Extended section of **3** showing the combination of cation–π and agostic Rb–C interactions leading to the 2D sheet assembly. Hydrogen atoms are omitted for clarity.

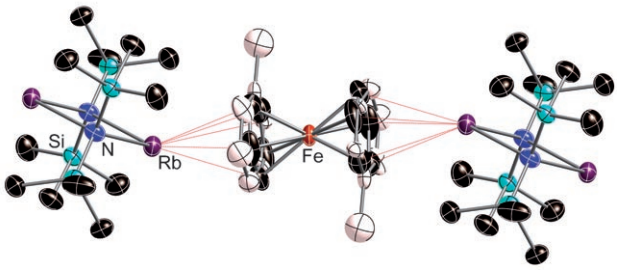

Figure 7. Section of the molecular structure of **5** showing the relative positions of the partially occupied ferrocene and toluene molecules.

As expected, the metrical parameters for the dimeric ring components of **5** and **6** are almost identical to their toluene-free analogues **4** and **5** (Table 1). The inclusion of both toluene and ferrocene within **5** and **6** allows direct comparisons of the cation–π bonding of alkali metals to either an arene molecule or a cyclopentadienyl complex within single structures. In both compounds the toluene is located marginally closer to the metal center than the Cp ring. In **5**, the Rb–$Cp_{centroid}$ distance is 3.323 Å, with Rb–C distances ranging from 3.507(6)–3.561(6) Å. In comparison, the Rb–$Tol_{centroid}$ distance is 3.214 Å, with Rb–C distances ranging from 3.369(7)–3.630(4) Å. In **6**, the Cs–$Cp_{centroid}$ distance is 3.396 Å, with Cs–C distances between 3.549(7)–3.667(6) Å. The Cs–$Tol_{centroid}$ distance is 3.315 Å, with Cs–C distances ranging from 3.530(5)–3.658(4) Å. At first glance it may be surprising to note that the Cs–$Tol_{centroid}$ distance in **6** is 0.14 Å shorter than that in $[\{(Me_3Si)_2NCs\}_2\cdot(Tol)]_\infty$ (**8**).[75] Each toluene molecule in **8** bridges between a pair of metal amide dimers, as opposed to binding a single metal center in **6**, leading to significant lengthening of the metal–arene contacts. Therefore, the cation–π distances in **6** likely provides better data for comparative studies.

The extended structures of **5** and **6** are also similar to **3** and **4**. Once again, the ferrocene is tilted out of the plane of the M_2N_2 dimeric ring, creating a one-dimensional zigzag

chain. The M-M-$Cp_{centroid}$ angle is 150.05° and 149.16° for **5** and **6**, respectively. The intra- and intermolecular M–$C_{(HMDS)}$ interactions are also similar to **3** and **4**. It is remarkable that the inclusion of toluene in **5** and **6** has such a minor effect on overall structures. All of the crystals **4**–**6** have the same space group ($P2_1/n$) and have very similar unit cell parameters (Experimental section, Table 5). Therefore, the extended structures of these mixed-solvate species are composed of metal–amide dimers that are either bridged through ferrocene or alternatively two adjacent dimers are terminally solvated by a pair of toluene molecules (Figure 8). Overall, the extended structures of **5** and **6** are two-dimensional 4^4-sheets assembled from combination of cation–π, agostic, and π–π interactions.

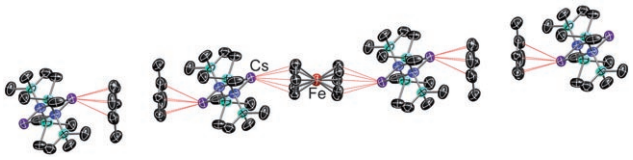

Figure 8. Section of the extended structure of **6** showing two alternative solvation modes within the crystal: i) bridging of the amide dimers by ferrocene (middle section) and ii) terminal binding of toluene on two adjacent dimers (end sections).

The structural substitution of ferrocene by a pair of toluene molecules is made feasible as the π–π stacking distance between the arenes is close to the Cp–Cp separation in ferrocene. Specifically, the centroid–centroid distances for two adjacent toluene molecules is 3.593 and 3.609 Å in **5** and **6**, respectively, with corresponding Cp–Cp distances of 3.386 and 3.327 Å. The separation of the toluene molecules lies within the range of 3.5–3.8 Å that has previously been calculated for face-to-face stacking for toluene.[78,79]

Computational studies: The interaction between alkali metal cations and aromatic systems has been the subject of numerous experimental and theoretical studies.[56,80–107] Of particular interest to our own work are the computational studies on the binding enthalpies of alkali metal cations to either toluene[93,102] or ferrocene.[56,91,105]

Ugalde and Wagner have recently reported the binding enthalpies of $M^+\cdots\eta^5$(ferrocene)[56b,91] complexes at the B3LYP/double-ζ (DZ) level of theory and compared these with the values obtained by Feller for the $M^+\cdots\eta^6$(benzene) complexes at the complete basis set limit (M^+ = Li, Na, K, Rb).[84] From this work it was concluded that all of the alkali metal cations establish relatively strong interactions with both ferrocene and benzene. The $M^+\cdots\eta^5$(ferrocene) binding enthalpies were calculated to be −44.0, −30.0, −20.1, and −14.8 kcal mol^{-1} for M^+ = Li, Na, K, and Rb respectively. This pattern is in accord with the cation–π interactions being predominantly electrostatic in nature.[3] In comparison, binding enthalpies for the $M^+\cdots\eta^6$(benzene) complexes were found to be −36.1, −24.2, −20.0, and −16.3 kcal mol^{-1} for M^+ = Li, Na, K, and Rb respectively. These values indicate that the smaller alkali metals form stronger cation–π contacts, and that ferrocene binding is substantially preferred over benzene for both Li and Na (by 7.9 and 5.8 kcal mol^{-1}, respectively). Increasing the size of the cation to K and Rb results in very similar binding enthalpies for ferrocene and benzene. It should be noted that the calculated binding enthalpies do vary somewhat depending on the computational method used and basis set chosen.[84,102,106]

There has been far less theoretical work studying the $M^+\cdots\eta^6$(toluene) interaction as compared to $M^+\cdots\eta^6$(benzene), but it is more relevant to our experimental work. Rodgers was the first to look at this interaction both theoretically and experimentally.[93] The calculated bond enthalpies (MP2(full)/6–311+G(2d,2p) basis set with BSSE corrections) gave similar values to that of benzene. However, the $M^+\cdots\eta^6$(toluene) bond enthalpies are weaker for all of the alkali metals when compared to the $M^+\cdots\eta^5$(ferrocene) enthalpies calculated by Ugalde and Wagner.[56] The $Li^+\cdots\eta^5$(ferrocene) and $Na^+\cdots\eta^5$(ferrocene) interactions are again highly favored by 6.8 and 6.5 kcal mol^{-1}, respectively, and both the $K^+\cdots\eta^5$(ferrocene) and $Rb^+\cdots\eta^5$(ferrocene) interactions are now slightly favored by 1.6 and 0.15 kcal mol^{-1}. Once again, these values can vary up to 3 kcal mol^{-1} based on the theoretical method and basis set used.[56,93,105]

We wished to supplement the previous calculations by studying the binding energies of ferrocene and toluene to the dimeric $[M(HMDS)]_2$ aggregates, in M = Li (**Ia**), Na (**IIa**), or K (**IIIa**), to give the disolvated complexes **I**–**III b** and **I**–**III c** (Scheme 1). To gain as complete a picture of steric effects as possible the full structures were geometry optimized by using the crystal data as starting positions. All calculations were carried out at the B3LYP/6–31G* level of theory with no constraints using the Gaussian 03 suite of programs.[108] Selected structural parameters are shown in Table 3.

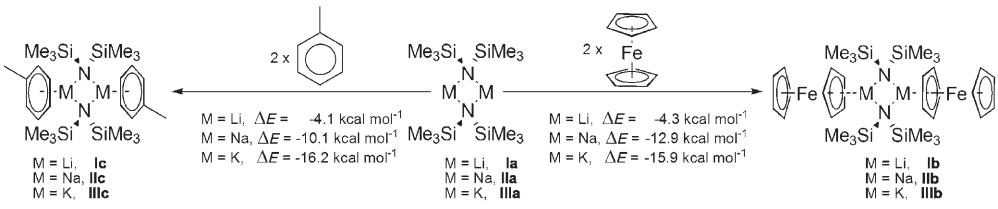

Scheme 1. Energetics of cation–π solvation for the metal amide dimers with ferrocene and toluene (B3LYP/6–31G*).

Table 3. Comparison of selected bond lengths [Å] and angles [°] for the calculated structures.

	M–N	Si–N	Si–C	N-M-N	M-N-M	Si-N-Si	M–Centroid	M-M-Centroid
Ia	1.981	1.724	1.899–	108.97	71.02	126.56	–	–
(M=Li)			1.925	111.15	71.04	126.60		
Ib	2.001–	1.732	1.904–	107.28	72.58	121.38	3.370	170.72
(M=Li)	2.006	1.737	1.913	107.33		121.39	3.379	170.81
Ic	1.981	1.727	1.893–	108.49	71.49	124.19	4.570	175.80
(M=Li)	1.987	1.729	1.920	108.53		124.89	4.577	176.95
IIa	2.347	1.717	1.904–	104.93	75.07	126.16	–	–
(M=Na)			1.925			126.19		
IIb	2.385–	1.716	1.908–	102.15	77.76	125.92	3.111	173.80
(M=Na)	2.390	1.717	1.917	102.25	77.77	126.44	3.133	173.82
IIc	2.377	1.714	1.905–	102.30	77.69	129.67	3.321	169.89
(M=Na)	2.431	1.715	1.916	102.33		129.74	3.327	169.91
IIIa	2.780	1.700	1.905–	96.31	83.69	132.62	–	–
(M=K)	2.781		1.921					
IIIb	2.822–	1.698	1.908–	95.80	84.18	132.62	3.151	177.99
(M=K)	2.827		1.921	95.83	84.19	132.64	3.152	177.92
IIIc	2.797	1.697	1.907–	94.93	85.07	133.23	3.210	175.15
(M=K)	2.862		1.922			133.24	3.211	175.17

First, the calculated metrical parameters for the dimeric M_2N_2 rings very accurately reproduce those seen in the relevant crystal structures. For example, the M–N distances of the unsolvated species **Ia**–**IIIa** are within 0.02 Å of their experimental analogues.[64,71,109] Furthermore, direct comparisons can be made between the calculated and experimental values for the unsolvated potassium amide dimer, as this compound has previously been crystallographically characterized.[71] Overall the bond lengths and angles vary by <0.04 Å and $<3.5°$, respectively, between theory and experiment.[71] This level of theory appears to be adequate to obtain reasonable geometries for these alkali-metal amide complexes.

The calculations involving LiHMDS, **Ib** and **Ic**, essentially resulted in expulsion of the arenes from the metal's coordination sphere. The average Li–$Cp_{centroid}$ distance in **Ib** is 3.375 Å with Li–C distances ranging between 2.867–4.272 Å. Also, the average Li–$Tol_{centroid}$ distance in **Ic** is 4.574 Å with Li–C distances between 4.530–5.009 Å. This corroborates our experimental studies, which showed that LiHMDS does not crystallize as a solvated complex with either ferrocene or toluene. The inability of ferrocene and toluene to interact with the lithium centers in **I** is clearly a consequence of steric congestion at the metal, since prior studies have already established that uncoordinated cation–π binding energies increase with decreasing size of the alkali metal.[56b] It should be noted that disolvated LiHMDS dimers are known, but these all involve interactions with smaller monodentate solvents such as ethers or amines.[110–115]

The calculations involving NaHMDS and KHMDS optimized to geometries in which both ferrocene and toluene coordinate to the metal cations (Figure 9). In **IIb**, the sodium centers η^2-coordinate to ferrocene, with shorter Na–C distances in the range 2.890–3.022 Å, and with longer Na–C distances ranging between 3.398–3.796 Å. The two Na–$Cp_{centroid}$ distances in **IIb** are 3.111 and 3.133 Å. Similarly, the two toluene molecules in **IIc** are η^2-coordinated by the sodium centers, with the shorter Na–C bonds lying between 3.060–3.083 Å and with the longer Na–C bonds in the range 3.580–4.102 Å. Also, the Na–$Tol_{centroid}$ distances are 3.321 and 3.327 Å, which are approximately 0.2 Å longer than those in **IIb**. The η^2-bonding in **IIb** differs from the η^5-bonding found in the crystal structure of **1**. However, a single-point energy calculation on the molecule with a fixed Na–$Cp_{centroid}$ distance of 3.12 Å and with the ferrocenes aligned in an η^5 fashion results in an increase of <1.3 kcal mol^{-1}, relative to the optimized geometry of **IIb**. So, the difference in energy between η^2 and η^5 bonding is small for the sodium–amide dimer. This is likely a consequence of remaining steric repulsions between the HMDS groups and the metallocene (although clearly less than in the lithium analogue). Furthermore, this analysis is consistent with the experimental finding that the mean sodium–Cp centroid distance in **1** is unexpectedly 0.22 Å longer than in the more highly solvated complex **10**.

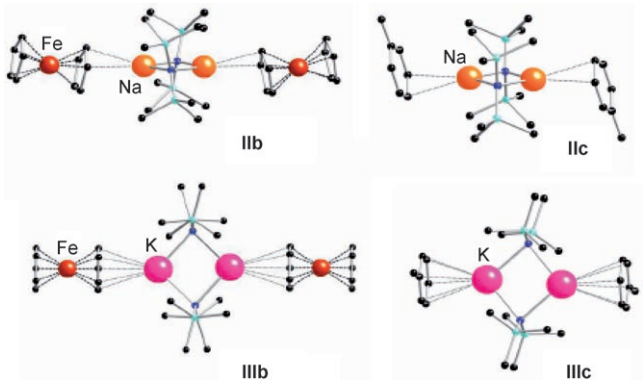

Figure 9. Geometry optimized structures of the cation–π solvated sodium and potassium amide dimers. Hydrogen atoms are omitted for clarity.

The two potassium atoms in **IIIb** η^5-coordinate to ferrocene, as was found in the crystal structure of **2**. The K–$Cp_{centroid}$ distances in **IIIb** are 3.151 and 3.152 Å, with K–C distances ranging between 3.370–3.387 Å. The toluene molecules in **IIIb** are η^6-coordinated by the potassium atoms, with K–C distances lying between 3.456–3.562 Å and K–$Tol_{centroid}$ distances of 3.210 and 3.211 Å. The ferrocene lies closer than toluene to potassium, which was also the case for the analogous sodium complexes **IIb**/**IIc**. The difference between the mean metal–centroid distances is now smaller at 0.06 Å compared with 0.20 Å between **IIb** and **IIc**. These results reflect those found experimentally, where the K–

$Cp_{centroid}$ distance in **2** is 0.05 Å shorter than the K–$Tol_{centroid}$ distance in **7**.

Considering the calculated binding energies shown in Scheme 1, it is seen that the cation–π interactions for both ferrocene and toluene strengthen with increasing size of the alkali metal. This is the opposite trend to that found for binding of the bare metal ions to the aromatic groups.[56,93,102,106] In this regard it is worth noting that the calculated binding energy of 16.2 kcal mol^{-1} for toluene to the potassium amide dimer is very similar to the value of 16.6 kcal mol^{-1} previously calculated for the bare metal cation.[102] Moreover, these results are in accord with the value of 19.1 kcal mol^{-1} determined experimentally by the threshold collision-induced dissociation of $K^+(Tol)_x$.[93] Therefore, the discrepancy in the relative strengths of binding in our systems may explained by the HMDS ligands exerting less steric influence on ligand coordination as the cations increase in size that is, the available space for arene coordination increases.

For the sodium systems the binding energy of ferrocene is higher than for toluene by 2.8 kcal mol^{-1}. On the other hand, the larger potassium systems are essentially thermoneutral, with a binding energy difference of only 0.3 kcal mol^{-1} in favor of toluene solvation. These results mirror those for the bare cations binding to toluene and ferrocene, for which the smaller metals have stronger interactions with ferrocene, whereas the larger metals show little distinction between the aromatic groups.[56,93,102] Furthermore, the similarity in bond enthalpies for the larger metals is given experimental support by our characterization of the mixed toluene/ferrocene compounds **5** and **6**. For the smaller alkali-metal amides (M = Na, K), a combination of the larger energetic affinity for ferrocene over toluene, coupled with the limited coordination sphere available for interaction due to the presence of the sterically demanding HMDS groups give rise to the formation of the ferrocene-only compounds **1** and **2**. With the larger alkali metals amides (M = Rb, Cs) the binding energies are similar for ferrocene and toluene,[56,93,102] but steric crowding is less of an issue, resulting in the formation of the mixed toluene/ferrocene compounds **5** and **6**. This analysis is also consistent with our experimental finding that changing the solvent of crystallization from toluene to sterically more demanding *tert*-butylbenzene allows the crystallization of the pure ferrocene solvated rubidium and cesium compounds **3** and **4**.

Frequency analysis of the calculated structures indicated that they each adopt a true energy minimum. Additionally, this also allowed a comparison between the calculated and experimentally derived IR frequencies for this set of compounds. Table 4 lists selected experimental IR frequencies from **1**–**4**, ferrocene and the uncomplexed metal amides, as well as the calculated frequencies for **IIa**, **IIb**, **IIIa**, and **IIIb** (normalized values of the peaks from the predicted spectra). The quoted B3LYP/6–31G* calculated frequencies were scaled by a factor of 0.9614 to obtain comparable values with those found experimentally.[116] In general, reasonable agreement is found between the experimental and calculated data. No consistent pattern can be discerned for the $(Me_3Si)_2N^-$ units, but analysis of the ferrocene frequencies is more useful. In particular, small but consistent movements of 1–12 cm^{-1} are found upon complexation of ferrocene to the metal–amide dimers. This effect is most clearly seen in the ν(C-C) and the ring deformations. The experimental data shows decreases of 2–6 cm^{-1} for these vibrations upon complexation. Moreover, the calculated spectra for **IIb** and **IIIb** show two signals in this region, one for the non-coordinated Cp ring, which has a similar frequency to free ferrocene, and a second for the metal-bound Cp, for which the frequencies are lowered by 10–12 cm^{-1}. Overall, these data indicate that participation in cation–π interactions has a small, but noticeable effect on the bonding within the ferrocene moiety, which is consistent with our crystal structure analyses.

Characterization of a bis(benzene)chromium polymer: An unexpected discovery relating to this work was made during

Table 4. Selected experimental and calculated IR data [cm^{-1}].

	$\{(CH_3)_3Si\}_2N^-$			Cp_2Fe					
	δ(C–H)	ν_{as}(Si-N-Si)	ν_s(Si-N-Si)	ν(C–H)	ν(C–C)	ring def.	δ(C–H)	ring tilt	ν(Fe–ring)
experimental values									
$C_{10}H_{10}Fe$				3095	1407	1106	1000	492	478
$(Me_3Si)_2NNa$	1305	1035	574						
$[\{(Me_3Si)_2NNa\}_2{\cdot}(Cp_2Fe)]_\infty$ (**1**)	1305	1062	575	3100	1403	1101	1004	494	481
$(Me_3Si)_2NK$	1304	1087	559						
$[\{(Me_3Si)_2NK\}_2{\cdot}(Cp_2Fe)]_\infty$ (**2**)	1303	1078	561	3100	1405	1100	1004	494	481
$(Me_3Si)_2NRb$	1303	1099	557						
$[\{(Me_3Si)_2NRb\}_2{\cdot}(Cp_2Fe)]_\infty$ (**3**)	1303	1091	565	3099	1405	1102	1004	495	479
$(Me_3Si)_2NCs$	1302	1099	553						
$[\{(Me_3Si)_2NCs\}_2{\cdot}(Cp_2Fe)]_\infty$ (**4**)	1301	1102	561	3098	1405	1102	1004	497	479
theoretical values									
$C_{10}H_{10}Fe$				3131	1413	1097	996	491	461
$[(Me_3Si)_2NNa]_2$ (**IIa**)	1267, 1258	1009	542						
$[\{(Me_3Si)_2NNa\}_2{\cdot}2(Cp_2Fe)]$ (**IIb**)	1272, 1261	1013	540	3133	1415, 1405	1097, 1087	996	493	461
$[(Me_3Si)_2NK]_2$ (**IIIa**)	1271, 1257	1065	519						
$[\{(Me_3Si)_2NK\}_2{\cdot}2(Cp_2Fe)]$ (**IIIb**)	1268, 1254	1070	517	3134	1415, 1403	1097, 1087	996	493	461

studies focused on the development of heterodimetallic amide reagents.[117] Mixed alkali/alkaline earth metal amide bases have been shown to possess remarkable selectivity in the deprotonation of aromatic substrates, including the regioselective 1,1′,2,2′-tetrametalation of ferrocene,[118] and the monometalation of both bis(benzene)chromium[119] and bis(toluene)chromium.[120] The bases used in these instances are derived from the alkyl amides 2,2,6,6-tetramethylpiperidide or diisopropylamide. Substitution by the weaker base hexamethyldisilazide may result in complex formation rather than deprotonation, as evidenced by the characterization of the previously mentioned molecular complex $[K\cdot(Cp_2Fe)_2\cdot(Tol)_2]^+[Mg(HMDS)_3]^-$ (**9**).[53] Replacement of ferrocene by bis(benzene)chromium has the effect of creating the polymer $[\{K\cdot((C_6H_6)_2Cr)_2\}^+\{Mg(HMDS)_3\}^-]_\infty$ (**14**).[119] The structure of **14** has each potassium center solvated by one terminal and two bridging bis(benzene)chromium molecules, to produce a one-dimensional chain.

A new variant of this complex $[\{K\cdot((C_6H_6)_2Cr)_{1.5}\cdot(Mes)\}^+\{Mg(HMDS)_3\}^-]_\infty$ (**15**) was prepared on carrying out a similar reaction in the presence of mesitylene. As can be seen in Figure 10, compound **15** contains magnesium tris(amide) anions and potassium cations that are coordinated to a mesitylene and three bis(benzene)chromium molecules. The mesitylene is η^6-coordinated to the potassium with K–C distances in the range 3.244–3.330 Å, whereas the metallocenes are best described as η^3-coordinated, with shorter K–C distances in the range 3.249–3.393 Å, and longer distances between 3.445–3.756 Å. Overall, the K–C distances are substantially longer than those within the ferrocene complex **2**, but this comparison is not particularly useful due to the change in hapticity between the complexes.

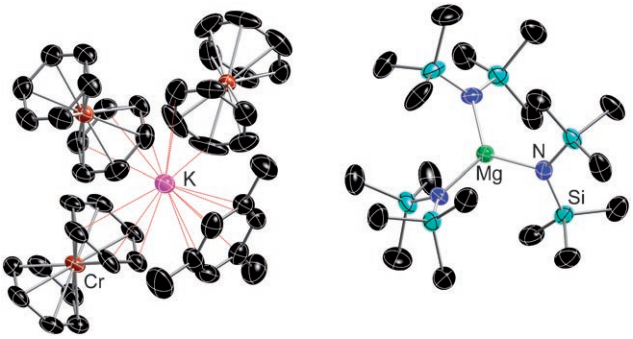

Figure 10. Section of the polymeric structure of **15** showing the charge-separated potassium cation and the magnesium tris(amide)amide anion. Hydrogen atoms are omitted for clarity.

The extended structure of **15** proves to be interesting. Whereas the mesitylene simply terminally solvates the metal center, all three of the bis(benzene)chromium molecules bridge to neighboring potassium cations. In effect the metal centers act as trigonal nodes to build two-dimensional 6^3-nets (Figure 11). The magnesium tris(amide) cations occupy the interstitial spaces between the ridged layers of adjacent sheets.

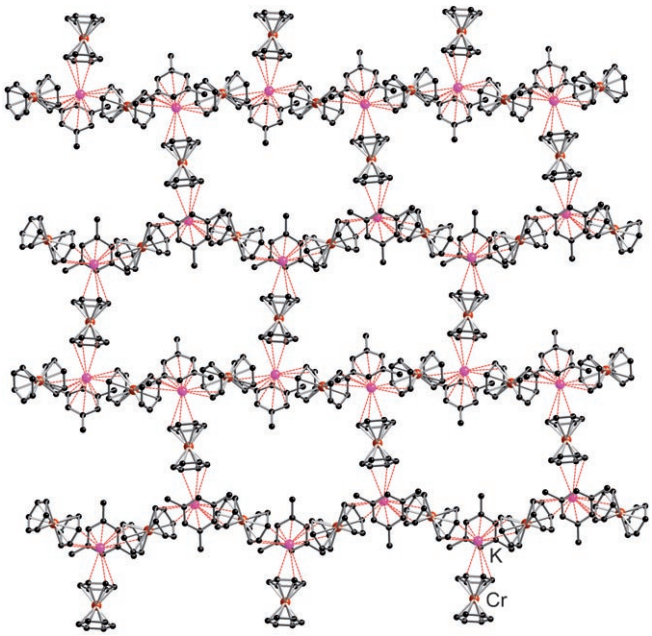

Figure 11. Section of the polymeric structure of **15** highlighting the 6^3-sheet formed by the trigonal potassium cation nodes and the bis(benzene)chromium bridges. The magnesium tris(amide) anions and hydrogen atoms are omitted for clarity.

The structure of **15** is noteworthy in that it is the first example of a two-dimensional cation–π network composed of entirely neutral bridging units. In this regard, bis(benzene)chromium provides a useful transition between simple arenes and cyclopentadienyl-based metallocenes for further studies of cation–π interactions.

Conclusion

Our studies confirm that ferrocene can be used as a ditopic linker to create extended networks through the use of cation–π interactions. The solid-state structural studies of **1**–**4** reveal that the combination of M(HMDS) (M = Na, K, Rb, Cs) with ferrocene gives rise to one-dimensional polymeric chains of dimeric ring amides bridged through ferrocene. In addition, **3** and **4** have close intermolecular agostic interactions with neighboring chains, such that the supramolecular structures may be considered as two-dimensional 4^4-nets.

Reaction of RbHMDS and CsHMDS with ferrocene in toluene media results in crystallization of the mixed toluene/ferrocene complexes **5** and **6**. The extended network topologies of **5** and **6** mirror those of **3** and **4**, but are now composed of an unusual combination of cation–π, agostic, and π–π interactions.

The solution studies used (NMR, UV/Vis and cryoscopy) were unable to detect the retention of ferrocene–cation contacts on dissolution of the crystalline polymers. This is not surprising as these interactions are likely to be highly labile in solution. Nevertheless, the solid-state IR and crystallo-

graphic studies indicate that participation in cation–π interactions does have noticeable effects on the bonding within the metallocene. Future work will focus on the photophysical and magnetic properties of such directionally ordered materials.[121]

Our calculations indicate that the strength of solvation by both ferrocene and toluene increases in the sequence Li < Na < K. However, this pattern is governed by the ability of the aromatic systems to enter the coordination sphere of the metals rather than representing the relative binding energies for simple cation–π contacts. These results demonstrate the importance of accurately modeling potential steric influences in order to obtain meaningful energetic information for cation–π interactions.

Both the experimental and theoretical studies consistently show shorter contacts between the sodium and potassium metal centers to ferrocene compared with toluene (≈0.1–0.2 Å). In comparison, almost identical distances are found between the metal centers and the ferrocene and toluene molecules in the mixed-solvate structures of **5** (Rb) and **6** (Cs). It appears that ferrocene is a stronger cation–π donor than toluene for the lighter alkali metals, but that this preference is removed on descending the group.

Characterization of the bis(benzene)chromium complex **15** shows that higher dimensionality polymers may be prepared through cation–π interactions, and that entirely neutral arene-based metallocenes may used in network formation.

The self-assembly of organometallic coordination networks is an emerging area, with the most comprehensive work to date completed by Sweigart on transition-metal quinonoid systems.[122] In these instances a variety of functional polymers have been assembled using organic linkers with pendant metals. The present work demonstrates that organometallic polymers may also be prepared in which the metals are integral components of the network itself. Studies are presently underway to investigate the use of various s-block aggregates and metallocene linkers to synthesize extended networks which adopt higher complexity topologies.

Experimental Section

General procedures: All experimental manipulations were performed under a dry nitrogen atmosphere by using standard Schlenk techniques, or in an argon-filled glovebox.[123] All glassware was flame-dried under vacuum before use. Toluene was dried immediately before use by passage through columns of copper-based catalyst and alumina (Innovative Technology), and stored over 4 Å molecular sieves. Mesitylene was distilled over CaH_2 prior to use. Bis(benzene)chromium was prepared by the literature method.[124] Ferrocene was purchased from Aldrich and sublimed under vacuum prior to use. NaHMDS and KHMDS were purchased from Alfa Aesar and Aldrich, respectively, and were used as received. *tert*-Butylbenzene was purchased from Aldrich and dried by storage over 4 Å molecular sieves. RbHMDS and CsHMDS were prepared according to literature procedures.[125] Deuterated solvents were purchased from Cambridge Isotope Laboratories and were dried by storage over 4 Å molecular sieves. ^{1}H and ^{13}C NMR spectra were recorded on either a Varian Unity Plus 300 MHz or a Bruker AVANCE DPX-400 spectrometer at 293 K, and were referenced internally to the residual signals of the deuterated solvents. The t_1 delay for the ^{1}H NMR experiments was set at 20 s in order to obtain accurate integration values for the cyclopentadienyl groups. Elemental analysis (C,H,N) was carried out on **1**–**6** by Midwest Microlab, LLC. Accurate analyses proved problematic due to the high moisture sensitivity of the compounds. However, powder diffraction on the bulk samples of **1**–**4** matched the theoretical powder patterns generated from the corresponding single-crystal data.

IR spectroscopic analysis: IR spectra were recorded on a Perkin–Elmer Paragon 1000 FTIR spectrometer. Samples were prepared as Nujol mulls using KBr plates. Selected peaks are listed Table 4 along with the calculated intensities taken from the frequency analysis of the optimized geometries of the calculated structures. The quoted infra-red frequencies were scaled by a factor of 0.9614.[116]

Computational details: The Gaussian 03 series of programs was used for the geometry optimization calculations.[108] No symmetry constraints were imposed and the molecules were allowed to freely optimize at the B3LYP/6–31G* level using related crystal structure data as starting geometries. The geometries were verified as true minima using frequency analyses.

X-ray crystallography: Crystals were examined under Infineum V8512 oil. The datum crystal was affixed to a thin glass fiber mounted atop a tapered copper mounting-pin and transferred to the 100 K nitrogen stream of a Bruker APEX II diffractometer equipped with an Oxford Cryosystems 700 series low-temperature apparatus. Cell parameters were determined by using reflections harvested from three sets of twenty 0.3° ω scans. The orientation matrix derived from this was passed to COSMO to determine the optimum data collection strategy.[126] Cell parameters were refined using reflections with $I \geq 10\sigma(I)$ harvested from the entire data collection. All data were corrected for Lorentz and polarization effects, as well as for absorption. Table 5 lists the key crystallographic parameters for **1**–**6** and **15**. The structures were solved and refined using SHELXTL.[127] Structure solution was by direct methods. Non-hydrogen atoms not present in the direct methods solution were located by successive cycles of full-matrix least-squares refinement on F^2. All non-hydrogen atoms were refined with parameters for anisotropic thermal motion. Hydrogen atoms were placed at idealized geometries and allowed to ride on the position of the parent atom. Hydrogen thermal parameters were set to 1.2× the equivalent isotropic U of the parent atom, 1.5× for methyl hydrogen atoms. CCDC-635034–635039 and 635859 contain the supplementary crystallographic data for this paper. These data can be obtained free of charge from The Cambridge Crystallographic Data Centre via www.ccdc.cam.ac.uk/data_request/cif.

Preparation and characterization

$[\{(Me_3Si)_2NNa\}_2\cdot(Cp_2Fe)]_\infty$ (1): Ferrocene (2.5 mmol, 465 mg) was added to a stirred solution of NaHMDS (5 mmol, 917 mg) in toluene (11 mL). A yellow precipitate formed, which completely dissolved on heating the solution to reflux temperature. X-ray quality crystals were obtained by slowly cooling the resulting solution in a hot water bath. Crystalline solid: yield 250 mg, 67.8%; ^{1}H NMR ([D$_6$]benzene, 293 K): $\delta = 0.08$ (s, 18H; Si(CH$_3$)$_3$), 3.98 ppm (s, 5H; Cp); ^{13}C NMR ([D$_6$]benzene, 293 K): $\delta = 6.87$ (Si(CH$_3$)$_3$), 68.24 ppm (Cp); m.p. 150 °C (decomp).

$[\{(Me_3Si)_2NK\}_2\cdot(Cp_2Fe)]_\infty$ (2): Ferrocene (1 mmol, 186 mg) was added to a stirred solution of KHMDS (2 mmol, 400 mg) in toluene (6 mL). The orange solution was filtered through Celite to remove a small amount of insoluble orange precipitate, followed by cooling the filtrate to 10 °C. X-ray quality crystals formed within 15 h. Crystalline solid: yield 370 mg, 96.1%. ^{1}H NMR ([D$_6$]benzene, 293 K): $\delta = 0.14$ (s, 18H; Si(CH$_3$)$_3$), 4.00 ppm (s, 5H; Cp); ^{13}C NMR ([D$_6$]benzene, 293 K): $\delta = 7.53$ (Si(CH$_3$)$_3$), 68.62 ppm (Cp); m.p. 150 °C (decomp).

$[\{(Me_3Si)_2NRb\}_2\cdot(Cp_2Fe)]_\infty$ (3): Ferrocene (1 mmol, 0.186 g) was added to a stirred solution of RbHMDS (2 mmol, 490 mg) in *tert*-butylbenzene (6 mL). The orange solution was cooled to −20 °C. X-ray quality crystals formed within 12 h. Crystalline solid: yield 400 mg, 92.8%; ^{1}H NMR ([D$_6$]benzene, 293 K): $\delta = 0.17$ (s, 18H; Si(CH$_3$)$_3$), 4.00 ppm (s, 5H; Cp); ^{13}C NMR ([D$_6$]benzene, 293 K): $\delta = 7.58$ (Si(CH$_3$)$_3$), 68.62 (Cp); m.p. 200 °C (decomp).

Table 5. Selected crystal data for **1–6** and **15**.

	1	**2**	**3**	**4**
formula	$C_{22}H_{46}FeN_2Na_2Si_4$	$C_{22}H_{36}FeK_2N_2Si_4$	$C_{22}H_{46}FeN_2Rb_2Si_4$	$C_{22}H_{46}Cs_2FeN_2Si_4$
M_r	552.80	574.94	677.76	772.64
T [K]	200(2)	200(2)	200(2)	200(2)
crystal system	orthorhombic	orthorhombic	monoclinic	monoclinic
space group	*Ccca*	*Fmmm*	$P2_1/n$	$P2_1/n$
a [Å]	14.664(3)	18.1618(3)	7.8880(4)	8.0580(2)
b [Å]	18.019(4)	14.7669(3)	17.7157(9)	17.6804(5)
c [Å]	11.956(2)	12.8125(2)	12.1361(6)	12.4615(4)
α [°]	90	90	90	90
β [°]	90	90	99.414(2)	98.986(1)
γ [°]	90	90	90	90
V [Å^3]	3159.1(11)	3436.23(10)	1673.08(15)	1753.58(9)
Z	4	4	2	2
ρ [Mg m^{-3}]	1.162	1.111	1.345	1.463
$\mu(Mo_{K\alpha})$ [mm^{-1}]	0.669	0.832	3.497	2.624
crystal size [mm]	0.35 × 0.28 × 0.26	0.43 × 0.37 × 0.32	0.45 × 0.55 × 0.35	0.47 × 0.35 × 0.22
θ range [°]	2.26–26.33	2.24–28.28	2.05–26.41	2.02–29.57
max/min transmission	0.8695/0.8109	0.8035/0.7116	0.3642/0.1991	0.5959/0.3687
reflns collected	18188	11756	31921	96709
independent reflns	1612	1194	3260	4907
observed reflns [$I > 2\sigma(I)$]	1447	1035	2642	4351
GOF on F^2	1.108	1.153	1.054	1.051
$R1$, $wR2$ [$I > 2\sigma(I)$]	0.0267, 0.0796	0.0322, 0.1140	0.0253, 0.0532	0.0236, 0.0501
$R1$, $wR2$ (all data)	0.0297, 0.0834	0.0369, 0.1205	0.0422, 0.0585	0.0293, 0.0532
largest peak/hole [e Å^{-3}]	0.245/−0.222	0.291/−0.251	0.408/−0.332	0.889/−0.755

	5	**6**	**15**
formula	$C_{23.62}H_{48.43}Fe_{0.6}N_2Rb_2Si_4$	$C_{24.02}H_{49.03}Cs_2Fe_{0.49}N_2Si_4$	$C_{90}H_{168}Cr_3K_2Mg_2N_6Si_{12}$
M_r	677.04	771.75	1954.20
T [K]	200 (2)	200(2)	123(2)
crystal system	monoclinic	monoclinic	orthorhombic
space group	$P2_1/n$	$P2_1/n$	*Pbcn*
a [Å]	8.030(2)	8.1328(3)	23.5979(7)
b [Å]	17.960(4)	17.7450(7)	31.3045(9)
c [Å]	12.450(3)	12.5957(5)	15.2979(4)
α [°]	90	90	90
β [°]	99.64(3)	98.567(2)	90
γ [°]	90	90	90
V [Å^3]	1770.2(6)	1797.49(12)	11300.9(6)
Z	2	2	4
ρ [Mg m^{-3}]	1.270	1.426	1.149
$\mu(Mo_{K\alpha})$ [mm^{-1}]	3.147	2.367	–
crystal size [mm]	0.44 × 0.38 × 0.30	0.41 × 0.22 × 0.15	0.4 × 0.15 × 0.10
θ range [°]	2.01- 28.36	2.00–30.50	2.91–26.37
max/min transmission	0.4552/0.2875	0.7149/0.4407	0.96/0.93
reflns collected	30211	41565	41398
independent reflns	4330	5431	11081
observed reflns [$I > 2\sigma(I)$]	3621	4845	7551
GOF on F^2	1.023	1.028	1.050
$R1$, $wR2$ [$I > 2\sigma(I)$]	0.0268, 0.0654	0.0252, 0.0593	0.0671, 0.1359
$R1$, $wR2$ (all data)	0.0380, 0.0702	0.0293, 0.0618	0.1087, 0.1551
largest peak/hole [e Å^{-3}]	0.689/−0.292	1.195/−0.759	0.754/−0.684

$[\{(Me_3Si)_2NCs\}_2\cdot(Cp_2Fe)]_\infty$ (4): Ferrocene (1 mmol, 0.186 g) was added to a stirred solution of CsHMDS (2 mmol, 586 mg) in *tert*-butylbenzene (4 mL). The orange solution was cooled to −20 °C. X-ray quality crystals formed within 12 h. Crystalline solid: yield 170 mg, 35.5 %; ^{1}H NMR ([D$_6$]benzene, 293 K): $\delta = 0.22$ (s, 18 H; Si(CH$_3$)$_3$), 4.00 ppm (s, 5 H; Cp); ^{13}C NMR ([D$_6$]benzene, 293 K): $\delta = 7.63$ (Si(CH$_3$)$_3$), 68.62 ppm (Cp); m.p. 180 °C (decomp).

$[\{(Me_3Si)_2NRb\}_2\cdot(Cp_2Fe)_{0.6}\cdot(C_7H_8)_{0.8}]_\infty$ (5): Ferrocene (1 mmol, 0.186 g) was added to a stirred solution of RbHMDS (2 mmol, 490 mg) in toluene (6 mL). The orange solution was cooled to −20 °C. X-ray quality crystals formed within 12 h. Crystalline solid: yield 220 mg, 51.04 %; ^{1}H NMR ([D$_6$]benzene, 293 K): $\delta = 0.09$ (s, 36 H; Si(CH$_3$)$_3$), 2.12 (s, 2.4 H; CH$_3$ toluene), 3.98 (s, 6 H; Cp), 7.08–7.12 ppm (s, 4 H; toluene, CH); ^{13}C NMR ([D$_6$]benzene, 293 K): $\delta = 7.15$ (Si(CH$_3$)$_3$), 68.22 (Cp); m.p. 180 °C (decomp).

$[\{(Me_3Si)_2NCs\}_2\cdot(Cp_2Fe)_{0.5}\cdot(C_7H_8)]_\infty$ (6): Ferrocene (1 mmol, 0.372 g) was added to a stirred solution of CsHMDS (2 mmol, 586 mg) in toluene (6 mL). The orange solution was cooled to −44 °C. X-ray quality crystals formed within 48 h. Crystalline solid: yield 350 mg, 73.0 %; ^{1}H NMR ([D$_6$]benzene, 293 K): $\delta = 0.09$ (s, 36 H; Si(CH$_3$)$_3$), 2.12 (s, 3 H; toluene CH$_3$), 3.99 (s, 5 H; Cp), 7.08–7.12 (s, 5 H; toluene, CH); ^{13}C NMR ([D$_6$]benzene, 293 K): $\delta = 5.67$ (Si(CH$_3$)$_3$), 68.17 ppm (Cp); m.p. 180 °C (decomp).

[K·{$(C_6H_6)_2Cr$}$_{1.5}$·(Mes)][{$(Me_3Si)_2N$}$_3$Mg] (15): Bu_2Mg (2 mL of a 1 M solution in heptane, 2 mmol) was diluted with 10 mL of hexane. HMDS(H) was then added (0.84 mL, 4 mmol) and the solution heated to reflux for 2 h. Upon cooling to ambient temperature KHMDS was then added (2 mmol, 4 mL), and the solution was heated to reflux for 1 h. After allowing to cool to ambient temperature bis(benzene)chromium (2 mmol, 0.42 g) was added followed by mesitylene (10 mL). The resulting mixture was heated to reflux for 1 h and allowed to slowly cool to ambient temperature. A crop of green, needle-shaped, crystals formed on standing. Crystalline solid: yield 0.91 g, 46.7%; ^{1}H NMR ([D$_8$]THF, 300 K): 6.74 (s, 3H; CH, Mes), 4.33 (s, 18H; $(C_6H_6)_2Cr$), 2.22 (s, 9H; CH_3, Mes), 0.07 ppm (s, 54H; $Si(CH_3)_3$); ^{13}C NMR ([D$_8$]THF, 300 K): $\delta = 127.8$ (CH, Mes), 75.2 ($(C_6H_6)_2Cr$), 25.6 (CH_3, Mes), 7.0 ppm ($Si(CH_3)_3$); m.p. 232–234 °C.

Acknowledgements

We gratefully acknowledge the Petroleum Research Fund (41716-AC3), Procter & Gamble, and the University of Notre Dame for support. We also thank the National Science Foundation for instrument support (CHE-0443233).

[1] N. S. Scrutton, A. R. C. Raine, *Biochem. J.* **1996**, *319*, 1–8.
[2] D. A. Dougherty, *Science* **1996**, *271*, 163–168.
[3] J. C. Ma, D. A. Dougherty, *Chem. Rev.* **1997**, *97*, 1303–1324.
[4] G. W. Gokel, S. L. De Wall, E. S. Meadows, *Eur. J. Org. Chem.* **2000**, 2967–2978.
[5] N. Zacharias, D. A. Dougherty, *Trends Pharmacol. Sci.* **2002**, *23*, 281–287.
[6] J. L. Sussman, M. Harel, F. Frolow, C. Oefner, A. Goldman, L. Toker, I. Silman, *Science* **1991**, *253*, 872–879.
[7] W. Zhong, J. P. Gallivan, Y. Zhang, L. Li, H. A. Lester, D. A. Dougherty, *Proc. Natl. Acad. Sci. USA* **1998**, *95*, 12088–12093.
[8] R. A. Kumpf, D. A. Dougherty, *Science* **1993**, *261*, 1708–1710.
[9] L. Heginbotham, Z. Lu, T. Abramson, R. MacKinnon, *Biophys. J.* **1994**, *66*, 1061–1067.
[10] D. A. Doyle, J. M. Cabral, R. A. Pfuetzner, A. Kuo, J. M. Gulbis, S. L. Cohen, B. T. Chait, R. MacKinnon, *Science*, **1998**, *280*, 69–77.
[11] J. P. Gallivan, D. A. Dougherty, *Proc. Natl. Acad. Sci. USA* **1999**, *96*, 9459–9464.
[12] P. C. Kearney, L. S. Mizoue, R. A. Kumpf, J. E. Forman, A. McCurdy, D. A. Dougherty, *J. Am. Chem. Soc.* **1993**, *115*, 9907–9919.
[13] S. Bartoli, S. Roelens, *J. Am. Chem. Soc.* **2002**, *124*, 8307–8315.
[14] H. S. Choi, S. B. Suh, S. J. Cho, K. S. Kim, *Proc. Natl. Acad. Sci. USA* **1998**, *95*, 12094–12099.
[15] a) G. W. Gokel, L. J. Barbour, S. L. De Wall, E. S. Meadows, *Coord. Chem. Rev.* **2001**, *222*, 127–154; b) E. S. Meadows, S. L. De Wall, L. J. Barbour, G. W. Gokel, *J. Am. Chem. Soc.* **2001**, *123*, 3092–3107; c) J. Hu, L. J. Barbour, G. W. Gokel, *J. Am. Chem. Soc.* **2001**, *123*, 9486–9487; d) G. W. Gokel, L. J. Barbour, R. Ferdani, J. Hu, *Acc. Chem. Res.* **2002**, *35*, 878–886.
[16] K. S. Oh, C.-W. Lee, H. S. Choi, S. J. Lee, K. S. Kim, *Org. Lett.* **2000**, *2*, 2679–2681.
[17] J. Chin, J. Oh, S. Y. Jon, S. H. Park, C. Walsdorff, B. Stranix, A. Ghoussob, S. J. Lee, H. J. Chung, S.-M. Park, K. Kim, *J. Am. Chem. Soc.* **2002**, *124*, 5374–5379.
[18] K. J. Thomas, R. B. Sunoj, J. Chandrasekhar, V. Ramamurthy, *Langmuir* **2000**, *16*, 4912–4921.
[19] E. Moret, J. Fürrer, M. Schlosser, *Tetrahedron* **1988**, *44*, 3539–3550.
[20] E. Masson, M. Schlosser, *Org. Lett.* **2005**, *7*, 1923–1925.
[21] S. Gowrisankar, K. Y. Lee, S. C. Kim, J. N. Kim, *Bull. Korean Chem. Soc.* **2005**, *26*, 1443–1446.
[22] P. C. Andrews, S. M. Calleja, M. Maguire, *J. Organomet. Chem.* **2005**, *690*, 4343–4348.
[23] R. G. Harrison, O. D. Fox, M. O. Meng, N. K. Dalley, L. J. Barbour, *Inorg. Chem.* **2002**, *41*, 838–843.
[24] Y. Li, C. M. Yang, *J. Am. Chem. Soc.* **2005**, *127*, 3527–3530.
[25] K. Konishi, T. Hiratani, *Chem. Lett.* **2006**, *35*, 184–185.
[26] H.-J. Schneider, L. Tianjun, N. Lomadze, *Eur. J. Org. Chem.* **2006**, 677–692.
[27] S. R. Batten, *CrystEngComm* **2001**, *18*, 67–72.
[28] B. H. Hong, S. C. Bae, C.-W. Lee, S. Jeong, K. S. Kim, *Science* **2001**, *294*, 348–351.
[29] a) D. J. MacDougall, J. J. Morris, B. C. Noll, K. W. Henderson, *Chem. Commun.* **2005**, 456–458; b) D. J. MacDougall, B. C. Noll, K. W. Henderson, *Inorg. Chem.* **2005**, *44*, 1181–1183; c) J. J. Morris, B. C. Noll, K. W. Henderson, *Cryst. Growth Des.* **2006**, *6*, 1071–1073; d) J. A. Rood, B. C. Noll, K. W. Henderson, *Inorg. Chem.* **2006**, *45*, 5521–5528; e) J. A. Rood, B. C. Noll, K. W. Henderson, *Main Group Chem.* **2006**, *5*, 21–31; f) D. J. MacDougall, B. C. Noll, A. R. Kennedy, K. W. Henderson, *Dalton Trans.* **2006**, 1875–1884; g) D. J. MacDougall, A. R. Kennedy, B. C. Noll, K. W. Henderson, *Dalton Trans.* **2005**, 2084–2091; h) K. W. Henderson, A. R. Kennedy, L. Macdonald, D. J. MacDougall, *Inorg. Chem.* **2003**, *42*, 2839–2841; i) K. W. Henderson, A. R. Kennedy, D. J. MacDougall, D. Shanks, *Organometallics* **2002**, *21*, 606–616.
[30] a) S. R. Batten, R. Robson, *Angew. Chem.* **1998**, *110*, 1558–1595; *Angew. Chem. Int. Ed.* **1998**, *37*, 1460–1494.
[31] A. J. Blake, N. R. Champness, P. Huberstey, W.-S. Li, M. A. Withersby, M. Schröder, *Coord. Chem. Rev.* **1999**, *183*, 117–138.
[32] D. Bragga, *J. Chem. Soc. Dalton Trans.* **2000**, 3705–3713.
[33] R. Robson, *J. Chem. Soc. Dalton Trans.* **2000**, 3735–3744.
[34] S. R. Batten, *Curr. Opin. Solid State Mater. Sci.* **2001**, *5*, 107–114.
[35] O. M. Yaghi, M. O'Keefe, N. W. Ockwig, H. K. Chae, M. Eddaoudi, J. Kim, *Nature* **2003**, *423*, 705–714.
[36] A. Y. Robin, K. M. Fromm, *Coord. Chem. Rev.* **2006**, *250*, 2127–2157.
[37] a) T. Takata, N. Kihara, Y. Furusho, *Adv. Polym. Sci.* **2004**, *171*, 1–75; b) T. Oku, Y. Furusho, T. Takata, *Angew. Chem.* **2004**, *116*, 984–987; *Angew. Chem. Int. Ed.* **2004**, *43*, 966–969.
[38] M. W. Hosseini, *Acc. Chem. Res.* **2005**, *38*, 313–323.
[39] a) G. R. Desiraju, *Crystal Engineering. The Design of Organic Solids*, Elsevier, Amsterdam, **1989**; b) G. R. Desiraju, *J. Chem. Soc. Dalton Trans.* **2000**, 3745–3751.
[40] A. D. Burrows, C.-W. Chan, M. M. Chowdhry, J. E. McGrady, D. M. P. Mingos, *Chem. Soc. Rev.* **1995**, *24*, 329–339.
[41] C. G. Claessens, J. F. Stoddart, *J. Phys. Org. Chem.* **1997**, *10*, 254–272.
[42] J. C. Noveron, B. Chatterjee, A. M. Arif, P. J. Stang, *J. Phys. Org. Chem.* **2003**, *16*, 420–425.
[43] C. Yue, Z. Lin, L. Chen, F. Jiang, M. Hong, *J. Mol. Struct.* **2005**, *779*, 16–22.
[44] O. Felix, M. W. Hosseini, A. De Cian, J. Fischer, *New J. Chem.* **1998**, *22*, 1389–1393.
[45] A. Ballabh, D. R. Trivedi, P. Dastidar, *Cryst. Growth Des.* **2005**, *5*, 1545–1553.
[46] A. M. Madalan, V. C. Kravtsov, Y. A. Simonov, V. Voronkova, L. Korobchenko, N. Avarvari, M. Andruh, *Cryst. Growth Des.* **2005**, *5*, 45–47.
[47] A. M. Ako, H. Maid, S. Sperner, S. H. H. Zaidi, R. W. Saalfrank, M. S. Alam, P. Mueller, F. W. Heinemann, *Supramol. Chem.* **2005**, *17*, 315–321.
[48] a) W. J. Hunks, M. C. Jennings, R. J. Puddephatt, *Inorg. Chem.* **1999**, *38*, 5930–5931; b) W. J. Hunks, M. C. Jennings, R. J. Puddephatt, *Inorg. Chem.* **2002**, *41*, 4590–4598.
[49] D. B. Leznoff, B.-Y. Xue, R. J. Batchelor, F. W. B. Einstein, B. O. Patrick, *Inorg. Chem.* **2001**, *40*, 6026–6034.
[50] C. Paraschiv, M. Andruh, S. Ferlay, M. W. Hosseini, N. Kyritsakas, J.-M. Planeix, N. Stanica, *Dalton Trans.* **2005**, 1195–1202.
[51] P. Metrangolo, G. Resnati, *Chem. Eur. J.* **2001**, *7*, 2511–2519.
[52] J. Fan, W.-Y. Sun, T. Okamura, Y.-Q. Zheng, B. Sui, W.-X. Tang, N. Ueyama, *Cryst. Growth Des.* **2004**, *4*, 579–584.
[53] G. W. Honeyman, A. R. Kennedy, R. E. Mulvey, D. C. Sherrington, *Organometallics* **2004**, *23*, 1197–1199.

[54] M. R. Haneline, F. P. Gabbaï, *Angew. Chem.* **2004**, *116*, 5587–5590; *Angew. Chem. Int. Ed.* **2004**, *43*, 5471–5474.
[55] S. Scholz, J. C. Green, H.-W. Lerner, M. Bolte, M. Wagner, *Chem. Commun.* **2002**, 36–37.
[56] a) A. H. Ilkhechi, M. Scheibitz, M. Bolte, H.-W. Lerner, M. Wagner, *Polyhedron* **2004**, *23*, 2597–2604; b) A. H. Ilkhechi, J. M. Mercero, I. Silanes, M. Bolte, M. Scheibitz, H.-W. Lerner, J. M. Ugalde, M. Wagner, *J. Am. Chem. Soc.* **2005**, *127*, 10656–10666; c) A. H. Ilkhechi, M. Bolte, H.-W. Lerner, M. Wagner, *J. Organomet. Chem.* **2005**, *690*, 1971–1977.
[57] D. R. Armstrong, R. Herbst-Irmer, A. Kuhn, D. Moncrieff, M. A. Paver, C. A. Russell, D. Stalke, A. Steiner, D. S. Wright, *Angew. Chem.* **1993**, *105*, 1807–1809; *Angew. Chem. Int. Ed. Engl.* **1993**, *32*, 1774–1776.
[58] C. Apostolidis, G. B. Deacon, E. Dornberger, F. T. Edelmann, B. Kanellakopulos, P. MacKinnon, D. Stalke, *Chem. Commun.* **1997**, 1047–1048.
[59] D. R. Armstrong, M. J. Duer, M. G. Davidson, D. Moncrieff, C. A. Russell, C. Stourton, A. Steiner, D. Stalke, D. S. Wright, *Organometallics* **1997**, *16*, 3340–3351.
[60] M. A. Beswick, H. Gornitzka, J. Kärcher, M. E. G. Mosquera, J. S. Palmer, P. R. Raithby, C. A. Russell, D. Stalke, A. Steiner, D. S. Wright, *Organometallics* **1999**, *18*, 1148–1153.
[61] A. D. Bond, R. A. Layfield, J. A. MacAllister, J. M. Rawson, D. S. Wright, M. McPartlin, *Chem. Commun.* **2001**, 1956–1957.
[62] R. A. Layfield, M. McPartlin, D. S. Wright, *Organometallics* **2003**, *22*, 2528–2530.
[63] For examples of cation–π complexes involving derivatized and/or heteroleptic metallocenes see: a) V. K. Bel'sky, Y. K. Gunko, B. M. Bulychev, A. I. Sizov, G. L. Soloveichik, *J. Organomet. Chem.* **1990**, *390*, 35–44; b) J. Hiller, V. Varga, U. Thewalt, K. Mach, *Collect. Czech. Chem. Commun.* **1997**, *62*, 1446- 1456; c) V. Varga, J. Hiller, U. Thewalt, M. Polá ek, K. Mach, *J. Organomet. Chem.* **1998**, *553*, 15–22; d) Z. Hou, Y. Zhang, H. Tezuka, P. Xie, O. Tardif, T. Koizumi, H. Yamazaki, Y. Wakatsuki, *J. Am. Chem. Soc.* **2000**, *122*, 10533–10543; e) N. Feeder, A. D. Hopkins, R. A. Layfield, D. S. Wright, *J. Chem. Soc. Dalton Trans.* **2000**, 2247–2248; f) Y. Wang, Q. Shen, *Organometallics* **2000**, *19*, 357–360; g) W. Clegg, K. W. Henderson, A. R. Kennedy, R. E. Mulvey, C. T. O'Hara, R. B. Rowlings, D. M. Tooke, *Angew. Chem.* **2001**, *113*, 4020–4023; *Angew. Chem. Int. Ed.* **2001**, *40*, 3902–3905; h) E. Kirillov, L. Toupet, C. W. Lehmann, A. Razavi, S. Kahlal, J-Y. Saillard, J.-F. Carpentier, *Organometallics* **2003**, *22*, 4038–4046; i) P. C. Andrikopoulos, D. R. Armstrong, W. Clegg, C. J. Gilfillan, E. Hevia, A. R. Kennedy, R. E. Mulvey, C. T. O'Hara, J. A. Parkinson, D. M. Tooke, *J. Am. Chem. Soc.* **2004**, *126*, 11612–11620; j) M. T. Gamer, P. W. Roesky, *Inorg. Chem.* **2005**, *44*, 5963–5965.
[64] R. Gruning, J. L. Atwood, *J. Organomet. Chem.* **1977**, *137*, 101–111.
[65] J. Knizek, I. Krossing, H. Noth, H. Schwenk, T. Seifert, *Chem. Ber./ Recl.* **1997**, *130*, 1053–1062.
[66] M. Karl, G. Seybert, W. Massa, K. Harms, S. Agarwal, R. Maleika, W. Stelter, A. Greiner, W. Heitz, B. Neumüller, K. Dehnicke, *Z. Anorg. Allg. Chem.* **1999**, *625*, 1301–1309.
[67] F. T. Edelmann, F. Pauer, M. Wedler, D. Stalke, *Inorg. Chem.* **1992**, *31*, 4143–4146.
[68] G. C. Forbes, A. R. Kennedy, R. E. Mulvey, P. J. A. Rodger, *Chem. Commun.* **2001**, 1400–1401.
[69] K. W. Henderson, A. E. Dorigo, Q.-Y. Liu, P. G. Williard, *J. Am. Chem. Soc.* **1997**, *119*, 11855–11863.
[70] C. Knapp, E. Lork, T. Borrmann, W.-D. Stohrer, R. Mews, *Z. Anorg. Allg. Chem.* **2005**, *631*, 1885–1892.
[71] K. F. Tesh, T. P. Hanusa, J. C. Huffman, *Inorg. Chem.* **1990**, *29*, 1584–1586.
[72] P. G. Williard, *Acta Crystallogr. Sect. C* **1988**, *44*, 270–272.
[73] R. W. Alder, M. E. Blake, C. Bortolotti, S. Bufali, C. P. Butts, E. Linehan, J. M. Oliva, A. G. Orpan, M. J. Quayle, *Chem. Commun.* **1999**, 241–242.
[74] A. M. Domingos, G. M. Sheldrick, *Acta Crystallogr. Sect. B* **1974**, *30*, 517–519.
[75] S. Neander, U. Behrens, *Z. Anorg. Allg. Chem.* **1999**, *625*, 1429–1434.
[76] For other homologous series of alkali metal compounds see: a) S. T. Liddle, W. Clegg, *Polyhedron* **2003**, *22*, 3507–3513; b) D. R. Armstrong, W. Clegg, A. M. Drummond, S. T. Liddle, R. E. Mulvey, *J. Am. Chem. Soc.* **2000**, *122*, 11117–11124.
[77] P. Seiler, J. D. Dunitz, *Acta Crystallogr. Sect. B* **1975**, *35*, 2020–2032.
[78] C. Chipot, R. Jaffe, B. Maigret, D. A. Pearlman, P. A. Kollman, *J. Am. Chem. Soc.* **1996**, *118*, 11217–11224.
[79] A. L. Ringer, M. O. Sinnokrot, R. P. Lively, C. D. Sherrill, *Chem. Eur. J.* **2006**, *12*, 3821–3828.
[80] S. Hashimoto, S. Ikuta, *J. Mol. Struct. THEOCHEM* **1999**, *468*, 85–94.
[81] V. Ryzhov, R. C. Dunbar, *J. Am. Chem. Soc.* **1999**, *121*, 2259–2268.
[82] O. M. Cabarcos, C. J. Weinheimer, J. M. Lisy, *J. Chem. Phys.* **1999**, *110*, 8429–8435.
[83] P. B. Armentrout, M. T. Rodgers, *J. Phys. Chem. A* **2000**, *104*, 2238–2247.
[84] D. Feller, D. A. Dixon, J. B. Nicholas, *J. Phys. Chem. A* **2000**, *104*, 11414–11419.
[85] J. C. Amicangelo, P. B. Armentrout, *J. Phys. Chem. A* **2000**, *104*, 11420–11432.
[86] J. P. Gallivan, D. A. Dougherty, *J. Am. Chem. Soc.* **2000**, *122*, 870–874.
[87] M. T. Rodgers, P. B. Armentrout, *J. Am. Chem. Soc.* **2000**, *122*, 8548–8558.
[88] S. Ikuta, *J. Mol. Struct. THEOCHEM* **2000**, *530*, 201–207.
[89] A. Gapeev, R. C. Dunbar, *J. Am. Chem. Soc.* **2001**, *123*, 8360–8365.
[90] S. Tsuzuki, M. Yoshida, T. Uchimaru, M. Mikami, *J. Phys. Chem. A* **2001**, *105*, 769–773.
[91] A. Irigoras, J. M. Mercero, I. Silanes, J. M. Ugalde, *J. Am. Chem. Soc.* **2001**, *123*, 5040–5043.
[92] H. Huang, M. T. Rodgers, *J. Phys. Chem. A* **2002**, *106*, 4277–4289.
[93] R. Amunugama, M. T. Rodgers, *J. Phys. Chem. A* **2002**, *106*, 5529–5539.
[94] R. Amunugama, M. T. Rodgers, *J. Phys. Chem. A* **2002**, *106*, 9718–9728.
[95] J.-F. Gal, P.-C. Maria, M. Decouzon, O. Mó, M. Yánez, *Int. J. Mass Spectrom.* **2002**, *219*, 445–456.
[96] D. Kim, S. Hu, P. Tarakeshwar, K. S. Kim, J. M. Lisy, *J. Phys. Chem. A* **2003**, *107*, 1228–1238.
[97] W. Zhu, X. Tan, J. Shen, X. Luo, F. Cheng, P. C. Mok, R. Ji, K. Chen, H. Jiang, *J. Phys. Chem. A* **2003**, *107*, 2296–2303.
[98] F. M. Sui, N. L. Ma, C. W. Tsang, *Chem. Eur. J.* **2004**, *10*, 1966–1976.
[99] C. Ruan, M. T. Rodgers, *J. Am. Chem. Soc.* **2004**, *126*, 14600–14610.
[100] C. Garau, A. Frontera, D. Quinonero, P. Ballester, A. Costa, P. M. Deyà, *Chem. Phys. Lett.* **2004**, *392*, 85–89.
[101] W. Zhu, X. Luo, C. M. Puah, X. Tan, J. Shen, J. Gu, K. Chen, H. Jiang, *J. Phys. Chem. A* **2004**, *108*, 4008–4018.
[102] A. S. Reddy, G. N. Sastry, *J. Phys. Chem. A* **2005**, *109*, 8893–8903.
[103] C. Ruan, Z. Yang, N. Hallowita, M. T. Rodgers, *J. Phys. Chem. A* **2005**, *109*, 11539–11550.
[104] M. Güell, J. Poater, J. M. Luis, O. Mó, M. Yáñez, M. Solà, *ChemPhysChem* **2005**, *6*, 2552–2561.
[105] A. Frontera, D. Quinonero, C. Garau, P. M. Deyà, F. Pichierri, *Chem. Phys. Lett.* **2006**, *424*, 204–208.
[106] C. Coletti, N. Re, *J. Phys. Chem. A* **2006**, *110*, 6563–6570.
[107] M. Alberti, A. Aguilar, J. M. Lucas, F. Pirani, D. Cappelletti, C. Coletti, N. Re, *J. Phys. Chem. A* **2006**, *110*, 9002–9010.
[108] Gaussian 03, Revision C.01, M. J. Frisch, G. W. Trucks, H. B. Schlegel, G. E. Scuseria, M. A. Robb, J. R. Cheeseman, J. A. Montgomery, Jr., T. Vreven, K. N. Kudin, J. C. Burant, J. M. Millam, S. S. Iyengar, J. Tomasi, V. Barone, B. Mennucci, M. Cossi, G. Scalmani,

N. Rega, G. A. Petersson, H. Nakatsuji, M. Hada, M. Ehara, K. Toyota, R. Fukuda, J. Hasegawa, M. Ishida, T. Nakajima, Y. Honda, O. Kitao, H. Nakai, M. Klene, X. Li, J. E. Knox, H. P. Hratchian, J. B. Cross, V. Bakken, C. Adamo, J. Jaramillo, R. Gomperts, R. E. Stratmann, O. Yazyev, A. J. Austin, R. Cammi, C. Pomelli, J. W. Ochterski, P. Y. Ayala, K. Morokuma, G. A. Voth, P. Salvador, J. J. Dannenberg, V. G. Zakrzewski, S. Dapprich, A. D. Daniels, M. C. Strain, O. Farkas, D. K. Malick, A. D. Rabuck, K. Raghavachari, J. B. Foresman, J. V. Ortiz, Q. Cui, A. G. Baboul, S. Clifford, J. Cioslowski, B. B. Stefanov, G. Liu, A. Liashenko, P. Piskorz, I. Komaromi, R. L. Martin, D. J. Fox, T. Keith, M. A. Al-Laham, C. Y. Peng, A. Nanayakkara, M. Challacombe, P. M. W. Gill, B. Johnson, W. Chen, M. W. Wong, C. Gonzalez, J. A. Pople, Gaussian, Inc., Wallingford CT, **2004**.

[109] D. Mootz, A. Zinnius, B. Böttcher, *Angew. Chem.* **1969**, *81*, 398–399; *Angew. Chem. Int. Ed. Engl.* **1969**, *8*, 378–379.

[110] M. F. Lappert, M. J. Slade, A. Singh, J. L. Atwood, R. D. Rogers, R. Shakir, *J. Am. Chem. Soc.* **1983**, *105*, 302–304.

[111] R. P. Davies, *Inorg. Chem. Commun.* **2000**, *3*, 13–15.

[112] L. M. Engelhardt, B. S. Jolly, P. C. Junk, C. L. Raston, B. W. Skelton, A. H. White, *Aust. J. Chem.* **1986**, *39*, 1337–1345.

[113] K. W. Henderson, A. E. Dorigo, Q.-L. Liu, P. G. Williard, *J. Am. Chem. Soc.* **1997**, *119*, 11855–11863.

[114] G. C. Forbes, A. R. Kennedy, R. E. Mulvey, P. J. A. Rodger, R. B. Rowlings, *J. Chem. Soc. Dalton Trans.* **2001**, 1477–1484.

[115] P. G. Williard, Q.-Y. Liu, *J. Org. Chem.* **1994**, *59*, 1596–1597.

[116] A. P. Scott, L. Radom, *J. Phys. Chem.* **1996**, *100*, 16502–16513.

[117] R. E. Mulvey, *Organometallics* **2006**, *25*, 1060–1075.

[118] a) See reference [63g]; b) P. C. Andrikopoulos, D. R. Armstrong, W. Clegg, C. J. Gilfillan, E. Hevia, A. R. Kennedy, R. E. Mulvey, C. T. O'Hara, J. A. Parkinson, D. M. Tooke, *J. Am. Chem. Soc.* **2004**, *126*, 11612–11620.

[119] E. Hevia, G. W. Honeyman, A. R. Kennedy, R. E. Mulvey, D. C. Sherrington, *Angew. Chem.* **2005**, *117*, 70–74; *Angew. Chem. Int. Ed.* **2005**, *44*, 68–72.

[120] P. C. Andrikopoulos, D. R. Armstrong, E. Hevia, A. R. Kennedy, R. E. Mulvey, *Organometallics* **2006**, *25*, 2415–2418.

[121] T. J. Taylor, C. N. Burress, L. Pandey, F. P. Gabbai, *Dalton Trans.* **2006**, 4654–4656.

[122] a) M. Oh, G. B. Carpenter, D. A. Sweigart, *Acc. Chem. Res.* **2004**, *37*, 1–11; b) S. U. Son, J. A. Reingold , G. B. Carpenter, D. A. Sweigart, *Angew. Chem.* **2005**, *117*, 7888–7893; *Angew. Chem. Int. Ed.* **2005**, *44*, 7710–7715; c) S. U. Son, J. A. Reingold, D. A. Sweigart, *Chem. Commun.* **2006**, 708–710; d) S. U. Son, J. A. Reingold, G. B. Carpenter, P. T. Czech, D. A. Sweigart, *Organometallics* **2006**, *25*, 5276–5285; e) J. A. Reingold, M. Jin, D. A. Sweigart, *Inorg. Chim. Acta* **2006**, *359*, 2918–2923.

[123] D. F. Schriver, M. A. Drezdon, *The Manipulation of Air-Sensitive Compounds*, Wiley, New York, **1986**.

[124] E. O. Fischer, *Inorg. Synth.* **1960**, *6*, 132–137.

[125] F. T. Edelmann, F. Pauer, M. Wedler, D. Stalke, *Inorg. Chem.* **1992**, *31*, 4143–4146.

[126] J. Kaercher, COSMO, Bruker-Nonius AXS, Inc., Madison, Wisconsin, USA, **2003**.

[127] G. M. Sheldrick, University of Göttingen, Göttingen (Germany), **2001**.

Received: February 6, 2007
Published online: April 23, 2007

